

Heat Transfer and Fluid Flow Calculations of Industrial Shell Boilers and Evaluation of Operation Conditions – Draft

Saif-Aldain Aqel

2025

Contents

Abstract	3
1 Introduction	4
2 Industrial Application of Shell Boilers	7
2.1 Typical Industries	8
2.2 Standard Steam Duties	8
2.3 Advantages and Limitations	9
2.4 Multi-Pass Layout	10
3 Configuration	12
3.1 Layout	12
3.2 Geometry and surface specification	14
3.3 Assumptions and limitations	17
4 Combustion Model	18
4.1 Fuel and Air	19
4.1.1 Fuel Stream	19
4.1.2 Air Stream	19
4.1.3 Stoichiometric Oxygen requirement	20
4.1.4 Air-fuel ratio and excess air λ	21
4.2 Heating values and firing rate	22
4.2.1 HHV and LHV	22
4.2.2 Total heat input	24
4.3 Adiabatic flame temperature	24
4.4 Flue gas composition	26
5 Heat Transfer Model	28
5.1 Fundamental heat balance equations	28
5.2 Local energy balance	29
5.3 Overall conductance and resistance network	30
5.4 Wall temperature update and thermal convergence	31
5.5 Stage and boiler level duties	32
5.6 Gas side	33

5.6.1	Single tube and reversal chamber	34
5.6.2	Tube bank	35
5.6.3	Economizer	36
5.6.4	Radiation model	37
5.7	Water side	39
5.7.1	General formulation and boiling treatment	39
5.7.2	Economizer	43
5.7.3	Tube bank stages	45
5.7.4	Single tube and reversal chamber stages	46
6	Hydraulic Model	48
6.1	Frictional losses	48
6.2	Minor losses	50
6.3	Total pressure drop	51
6.4	Coupling of ΔP into the energy solver	51
7	Performance	52
7.1	solution procedure	52
7.2	Energy balance	53
7.3	Efficiency	53
7.4	Water/Steam flow rate convergence	54
7.5	Stage level performance	54
7.6	Boiler performance	55
8	Boiler performance analysis	56
8.1	Control case	56
8.2	Global boiler performance	57
8.3	Influence of excess air factor	58
8.4	Influence of fuel mass flow	60
8.5	Influence of drum pressure	62
8.6	Stage wise heat transfer behavior	64
8.7	Gas side hydraulics and heat transfer decomposition	65
9	Conclusion	67
A	config and input	69
A.1	Operating condition (<code>config/operation.yaml</code>)	69
A.2	Air input properties (<code>config/air.yaml</code>)	69
A.3	Fuel properties and composition (<code>config/fuel.yaml</code>)	69
A.4	Water input properties (<code>config/water.yaml</code>)	69
A.5	Drum geometry and wall properties (<code>config/drum.yaml</code>)	70
A.6	Heat exchanger stages (<code>config/stages.yaml</code>)	70
References		72

Abstract

This thesis develops a coupled combustion–heat transfer–hydraulics model for a three pass fire tube industrial shell boiler and evaluates its performance under realistic operating conditions. Implemented in Python, the modelling framework integrates (i) detailed fuel-air combustion, (ii) six sequential gas side heat exchange stages representing furnace radiation, convective tube banks, reversal chambers, and economizer, and (iii) a water/steam circuit governed by saturated boiling in the pressure parts and single phase heating in the economizer. The gas–water energy balance is solved using a one dimensional marching algorithm, which updates local heat transfer coefficients, wall temperatures, and segmental duties based on a full resistance network combining convection, radiation, fouling, and conduction.

Combustion calculations provide the adiabatic flame temperature, the fully burnt flue gas composition, and the total heat release from the lower heating value of the supplied natural gas fuel. Hydraulic losses are resolved concurrently using friction factor and minor loss correlations applied to each stage, yielding a complete gas side pressure drop profile. Boiler level performance metrics, including useful heat transfer, direct and indirect efficiencies, stack temperature, and the decomposition of radiative and convective duties, obtained after convergence of a fixed point iteration that links assumed efficiency to the resulting steam mass flow.

Sensitivity studies quantify the influence of excess air ratio, drum pressure, and firing rate on thermal performance, heat transfer distribution, pressure drop, and steam capacity. The results demonstrate that efficiency exhibits a shallow optimum near the design excess air setting; that pressure chiefly affects steam quantity rather than boiler efficiency; and that firing rate scales heat duties approximately linearly within the practical load range. The modelling framework provides a physics based tool suitable for analyzing industrial shell boiler behavior, supporting performance evaluation, operational optimization, and design exploration.

Chapter 1

Introduction

Industrial shell boilers remain one of the most widely deployed technologies for producing saturated steam and hot water in small to medium industrial plants. Their popularity arises from their compact construction, robust heat transfer surfaces, straightforward operation, and comparatively low installation and maintenance requirements. Typical applications span food and beverage processing, chemicals and pharmaceuticals, textiles, healthcare, and general manufacturing sectors where steady, reliable steam generation is essential for heating, processing, and auxiliary services.

Despite their apparent simplicity, the thermal behavior of shell boilers is governed by tightly coupled processes: multi stage radiative and convective heat transfer, natural circulation boiling inside the pressure parts, complex flue gas property variations, and geometry dependent hydraulic losses. Modern operation demands higher efficiency, reduced emissions, increased reliability, and improved control.

This thesis develops a physics based model for a three pass fire tube shell boiler that integrates combustion calculations, detailed flue gas thermophysical properties, multi stage heat transfer modelling, and hydraulic loss estimation. The model is implemented as a one dimensional marching solver applied to six sequential heat exchange stages:

$$\text{HX}_1 \rightarrow \text{HX}_2 \rightarrow \text{HX}_3 \rightarrow \text{HX}_4 \rightarrow \text{HX}_5 \rightarrow \text{HX}_6, \quad (1.1)$$

representing the furnace, reversal chambers, convective tube banks, and the economizer, see figure 1.1. On the water side, the boiler drum provides a saturated interface for nucleate boiling in the pressure parts, while the economizer section is treated as a single phase internal flow. Gas side properties are supplied by Cantera, enabling temperature dependent transport, specific heat, thermal conductivity, and radiative behavior to be modelled.

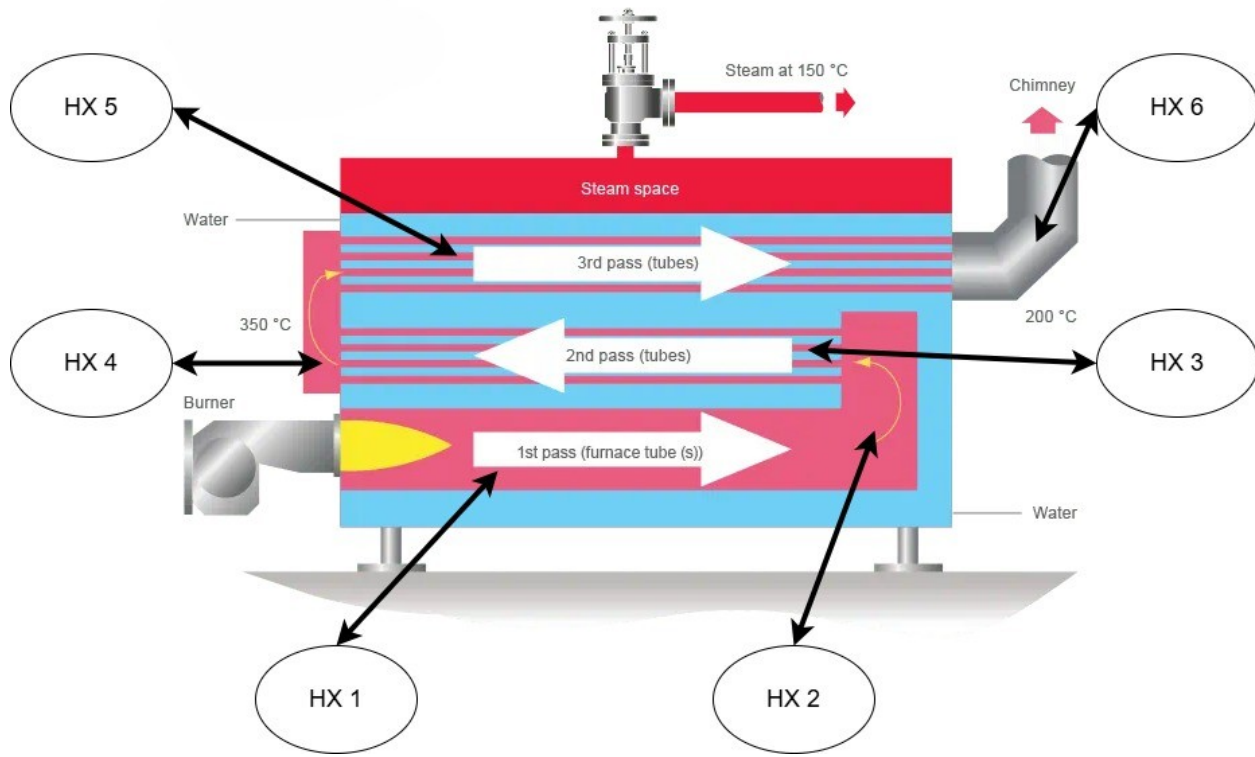


Figure 1.1: Shell boiler labeled stages.

The overall objectives of the study are:

1. To construct a unified combustion-boiler model capable of predicting flue gas temperature, composition, adiabatic flame temperature, and total heat input based on fuel composition and excess air settings.
2. To resolve heat transfer processes along the boiler using stage specific geometries, convection correlations, and a spectral based gas radiation model.
3. To quantify hydraulic losses across each pass using friction factor relations and minor loss coefficients, yielding the total boiler gas side pressure drop.
4. To compute boiler level performance, including useful heat transfer, direct and indirect efficiencies, stack temperature, and stage wise duties.
5. To evaluate sensitivity of boiler performance to key operating parameters, excess air ratio, drum pressure, and fuel mass flow rate.

The numerical framework is structured such that the water/steam mass flow is determined iteratively from the global energy balance. For each operating condition, a fixed point loop between assumed efficiency and resulting steam flow is solved until convergence, ensuring consistency between combustion input, heat transfer output, and steam generation.

The remainder of this thesis is organized as follows. Chapter 2 identifies typical industrial applications of shell boilers and introduces key design features. Chapter 3 describes the

boiler geometry and outlines the six heat transfer stages. Chapter 4 develops the combustion and flue gas model, including stoichiometry and adiabatic flame temperature prediction. Chapter 5 covers the heat transfer framework, combining convection and radiation on the gas side with pool boiling and single phase correlations on the water side. Chapter 6 presents the hydraulic model. Chapter 7 reports the resulting boiler performance, while Chapter 8 examines the sensitivity of the system to variations in λ , pressure, and firing rate. Chapter 9 concludes with a summary of findings.

Chapter 2

Industrial Application of Shell Boilers

Fire tube boilers- shell boilers

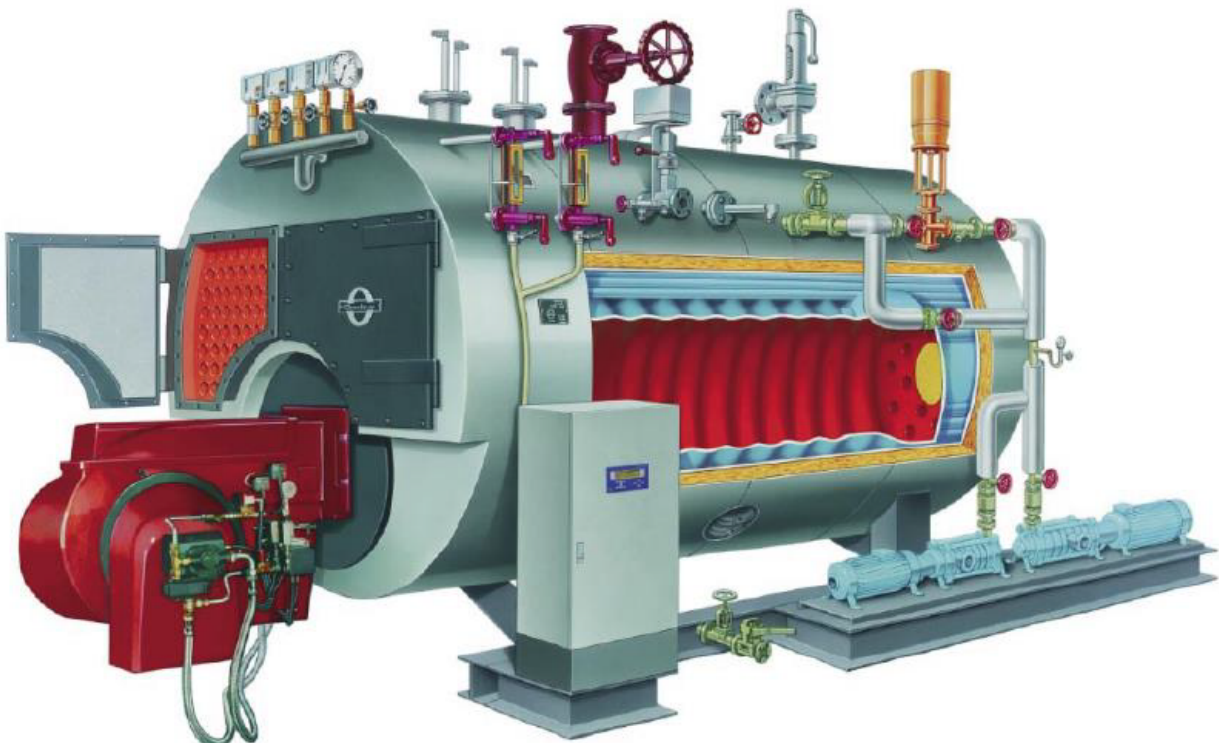


Figure 2.1: Example of a packaged fire tube shell boiler in industrial service.

2.1 Typical Industries

Shell (fire tube) boilers are widely used in small to medium steam and hot water duties where compactness, robustness, and simple operation are prioritized over very high pressure or very large throughput. Typical sectors include:

- Food and beverage
 - Breweries, dairies, sugar refineries
 - Canneries, bakeries, confectionery plants
 - CIP (clean-in-place) systems and sterilization
- Chemical and pharmaceutical
 - Fine chemicals, specialty chemicals
 - Active pharmaceutical ingredient (API) and formulation plants
 - Steam for reactors, jacket heating, and clean steam generators
- Textiles and paper
 - Dyeing, washing, drying, and calendaring operations
 - Small paper mills and converting facilities
- Healthcare and institutional
 - Hospitals, clinics, and laboratories (space heating, humidification, sterilizers, autoclaves)
 - Universities, office complexes, district heating sub-plants
- Light manufacturing and general industry
 - Metal finishing, surface treatment, and cleaning
 - Rubber and plastics processing
 - Laundry services and commercial dry-cleaning

2.2 Standard Steam Duties

Shell boilers are normally applied in low to medium pressure ranges and moderate steam capacities:

- Typical operating pressure range:
 - Saturated steam: 6–25 bar, occasionally up to 30 bar
 - Hot-water service: 10–16 bar
- Steam-generation rates (order of magnitude):
 - Small units: 0.5–5 t/h
 - Medium units: 5–20 t/h
 - Large shell boilers (upper practical range): 20–40 t/h, beyond which water-tube designs are usually preferred

2.3 Advantages and Limitations

Advantages

- Compact and integrated construction
 - Furnace, passes, and steam/water space are combined in a single pressure body.
 - Relatively small footprint and simple installation.
- Operational simplicity
 - Straightforward start-up and shutdown procedures.
 - Typically tolerant of moderate load swings and cycling (within design limits).
 - Often delivered as packaged units with burner, controls, and safety devices pre-engineered.
- Low-to-moderate capital cost
 - Attractive for small and medium plants, boiler houses, and decentralized steam supply.
- Good part-load performance
 - Large water content provides thermal buffer, reducing short-cycling of the burner.
 - Reasonable efficiency across a wide load range, especially with economizers.
- Maintenance and inspection
 - Accessible gas passes and tube bundles (depending on design) for cleaning and inspection.
 - Long-established technology with wide service and parts availability.

Limitations

- Pressure and capacity limits
 - Practical upper bounds on shell diameter and plate thickness limit maximum pressure and steam rate.
 - For very high pressure (e.g., >40–60 bar) or very large capacities, water-tube boilers are more suitable.
- Response time
 - Large water inventory slows thermal response to rapid, large load changes compared with water-tube boilers.
- Efficiency ceiling
 - Radiative and convective heat-transfer surfaces are constrained by geometry.

- Very high efficiencies often require additional heat-recovery equipment (economizers, condensing stages, air preheaters).
- Transport and installation constraints
 - Shell diameter and weight can be limited by route and lifting capacity.
 - Retrofitting within existing boiler houses may be constrained by overall envelope.

2.4 Multi-Pass Layout

Industrial shell boilers typically adopt multi-pass fire-tube configurations to enhance convective heat transfer and maintain acceptable gas-side velocities:

- Two-pass layout
 - First pass: large diameter furnace tube running from burner front to rear reversal chamber.
 - Second pass: return of flue gas through banks of small-diameter fire-tubes back to the front reversal chamber and flue outlet.
 - Simpler construction but lower total heat-transfer surface compared with three-pass designs.
- Three-pass layout (most common for industrial shell boilers)
 - Pass 1: large diameter furnace tube running from burner front to rear reversal chamber.
 - Pass 2: First bank of smoke-tubes (typically reversing at the rear turnaround chamber).
 - Pass 3: Second bank of smoke-tubes.
 - Provides higher overall heat-transfer surface, more uniform gas cooling, and lower exit-gas temperatures.
- Extended heat-recovery sections
 - Economizer: additional convective heat exchanger in the flue-gas path downstream of the boiler to preheat feedwater.
 - Air preheater / condensing sections: for high-efficiency systems using suitable fuels and materials.
- Flow arrangement
 - Gas-side: burner → furnace (Pass 1) → turnaround chamber → tube bank(s) (Passes 2 and 3) → stack.
 - Water/steam side: natural circulation between heated tube surfaces and the upper steam space within the drum/shell; feedwater introduced at cooler regions (often via economizer), steam drawn from the top of the shell.

This multi-pass concept underpins the subsequent detailed modelling of each convective and radiative heat-transfer stage HX_1 - HX_6 in the simulation.

Chapter 3

Configuration

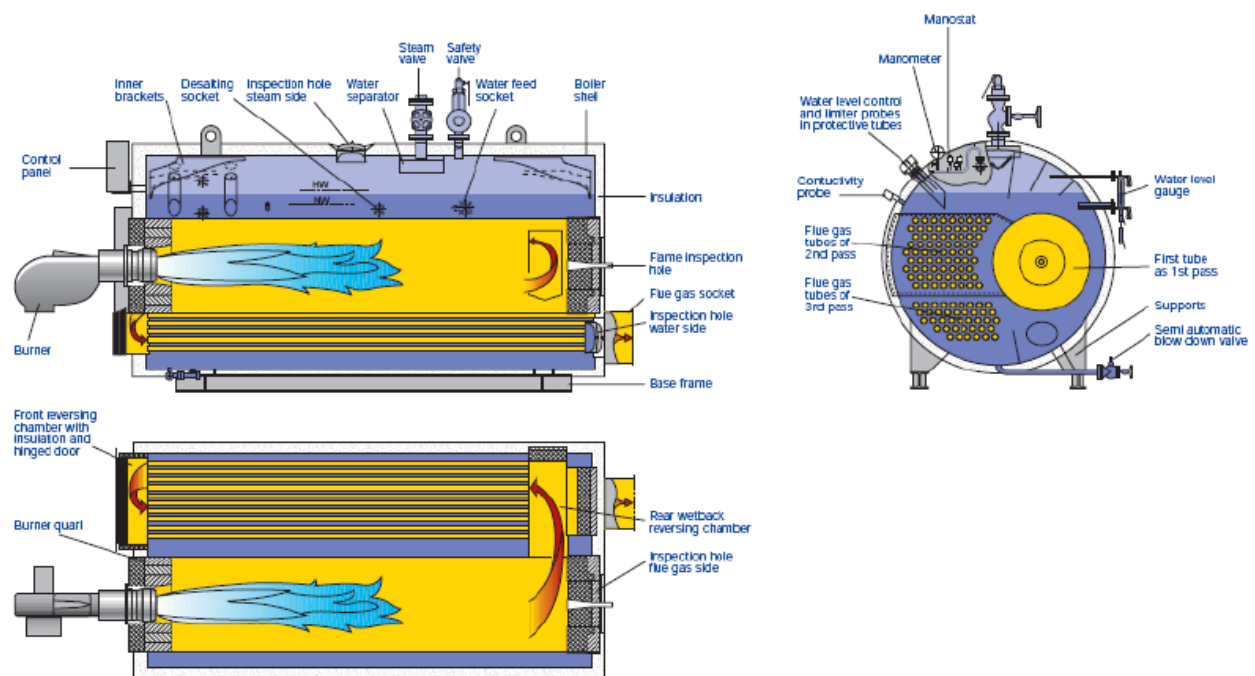


Figure 3.1: Example of shell boiler setup components

The simulated unit is a three pass fire tube shell boiler with six distinct gas side heat transfer stages and a single common steam drum on the water/steam side. Hot flue gas from the burner traverses a radiative furnace, two reversal chambers, two convective tube banks, and a final economizer before leaving to the stack.

3.1 Layout

The gas path is represented as:

$$\text{Burner} \rightarrow \text{HX}_1 \rightarrow \text{HX}_2 \rightarrow \text{HX}_3 \rightarrow \text{HX}_4 \rightarrow \text{HX}_5 \rightarrow \text{HX}_6 \rightarrow \text{stack} \quad (3.1)$$

with the following interpretation:

- HX_1 – Furnace (first pass)
Large, single furnace tube where combustion products enter directly from the burner and transfer heat mainly by radiation and high-temperature convection to the surrounding water/steam.
- HX_2 – First reversal chamber
Short cylindrical wet back chamber that turns the flow from the furnace outlet into the first convective tube bank (gas direction change = 180°).
- HX_3 – First convective tube bank (second pass) Bank of small diameter fire tubes arranged in a staggered pattern inside the shell, to boost convection; flue gas flows inside of the tubes, water/steam outside.
- HX_4 – Second reversal chamber Second turning chamber redirecting gas from the first to the second tube bank.
- HX_5 – Second convective tube bank (third pass) Second fire-tube bundle, representing the last in-boiler convective pass.
- HX_6 – Economizer Separate, downstream tube bank used to preheat feedwater in single-phase operation before entering the drum/boiler circuit, recovering heat, and boosting efficiency of the boiler.

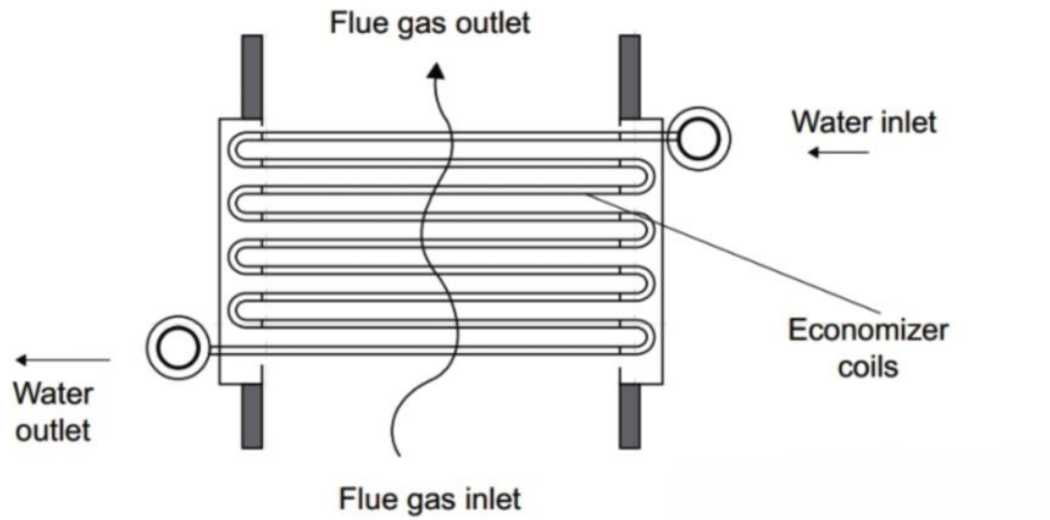


Figure 3.2: Cross-section of the economizer tube bundle HX_6 , showing gas-side cross-flow and water-side internal flow.

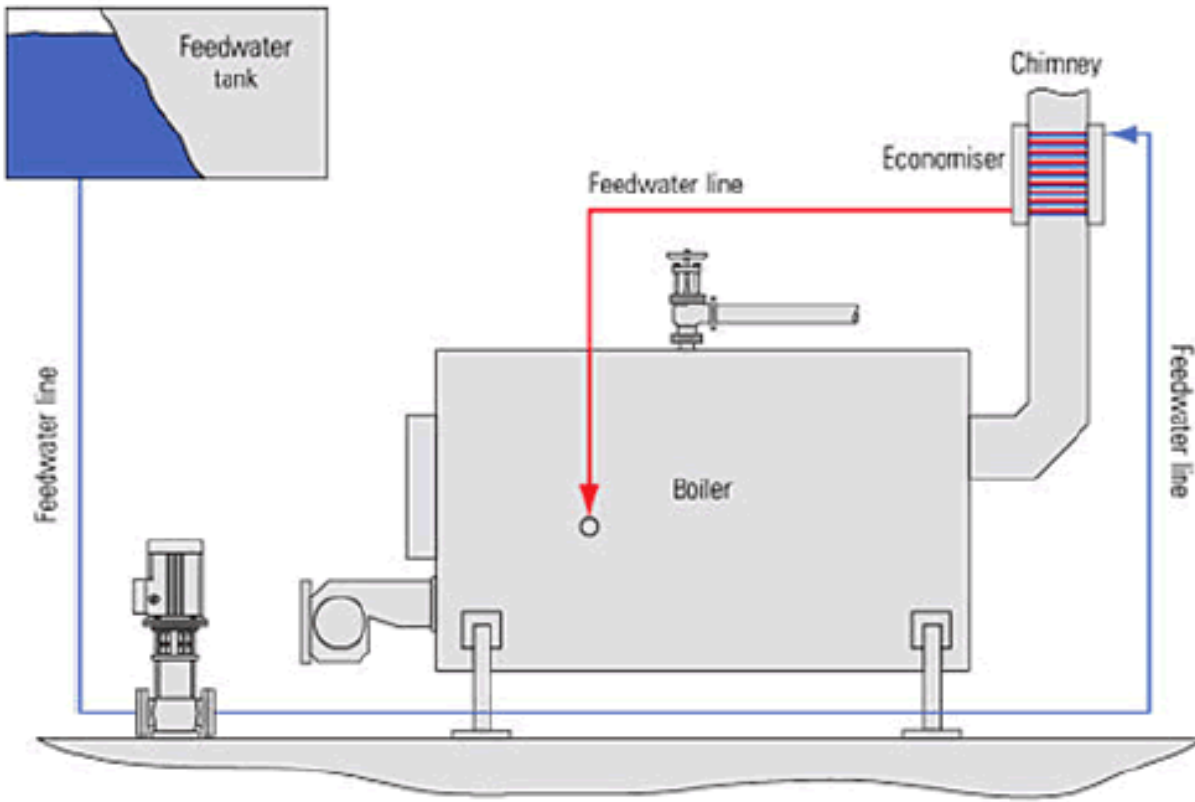


Figure 1: Economizer in Fire Tube Steam Boiler.

Figure 3.3: Three-pass shell boiler with rear-mounted economizer for feedwater preheating.

3.2 Geometry and surface specification

Drum configuration

The boiler has a single horizontal steam drum. Its inner diameter is $D_{i,\text{drum}} = 4.5 \text{ m}$ and its length $L_{\text{drum}} = 5.0 \text{ m}$.

The drum is not modelled with internal separators or circulation hardware. It simply supplies the saturated water/steam state at boiler pressure, while all circulation effects are represented by the single 1-D water/steam stream used in the heat-transfer stages.

Flue gas passes

All six pressure part stages of the simulated boiler are represented with a consolidated geometric and surface specification.

Table 3.1: Flue gas stages key parameters

Element	Kind	Di [m]	L [m]	N_tubes [-]	Wall t [mm]	Roughness [μm]	Pool boiling [-]
HX ₁	single_tube	1.40	5.276	1	2.9	0.5	true
HX ₂	reversal_ch.	1.60	0.80	1	2.9	0.5	true
HX ₃	tube_bank	0.076	4.975	118	2.9	0.5	true
HX ₄	reversal_ch.	1.60	0.80	1	2.9	0.5	true
HX ₅	tube_bank	0.076	5.620	100	2.9	0.5	true
HX ₆	economizer	0.076	7.50	160	2.5	0.5	false

The input file `stages.yaml`, provided in Annex A, contain the complete detailed specifications and is parsed at runtime by the configuration loader (`new_loader.py`). This separates numerical solution algorithms from geometry and surface data, and allows different boiler variants to be simulated by simply modifying the YAML files.

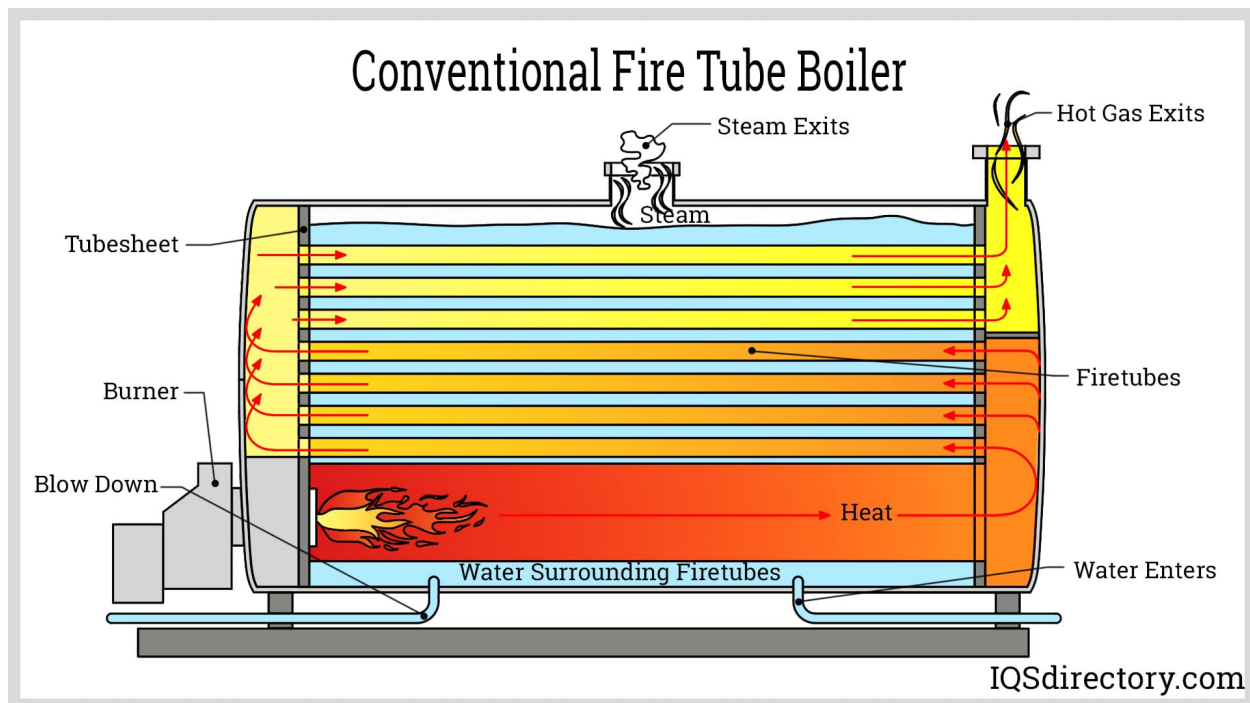


Figure 3.4: Detailed cross-section of the simulated boiler, showing drum, furnace, tube banks and reversal chambers.

All pressure part stages (HX_1 – HX_5) share the same steel wall thermal conductivity of $k_{\text{wall}} = 16 \text{ W/m/K}$. The economizer (HX_6) is modelled with a higher wall conductivity $k_{\text{wall}} = 30 \text{ W/m/K}$ and a clean surface (zero fouling thickness) to represent a best-case heat-recovery configuration.

The YAML configuration supplies wall, surface, and hydraulic properties not captured in the

tabulated geometry. Each pressure-part exchanger defines wall thickness, wall conductivity, surface roughness, emissivity, and optional fouling layers with specified thickness and conductivity. Most stages use a uniform carbon-steel wall with smooth surfaces and thin fouling layers, while the economizer uses a thinner, higher-conductivity wall and no fouling to reflect a cleaned section.

The steam drum defines diameter, length, and internal surface properties with its own roughness and fouling settings.

Reversal chambers specify curvature radius and nozzle minor-loss coefficients used in pressure-drop calculations.

Tube-bank stages define full shell-side layout: shell diameter, tube count and pitch, tube-row arrangement (staggered or inline), baffle spacing and cut, and bundle clearances. Evaporator banks use tighter pitch and spacing to enhance shell-side transfer, whereas the economizer uses a more open inline layout with a larger tube count and longer tubes.

These YAML entries are translated by the loader into the geometric and hydraulic quantities required for cross-flow areas, Reynolds numbers, and shell-side heat-transfer evaluation.

3.3 Assumptions and limitations

1. Combustion and flue gas

- Ideal complete combustion, with fixed excess air,
- Adiabatic flame temperature from equilibrium chemistry, using NASA polynomials.
- Ideal gas mixture $p = \rho RT$, with transport properties $\mu(T)$ $k(T)$ $c_p(T)$ from polynomial data.
- Steady state boiler operation, with fixed fuel air and feedwater.
- Boiler efficiency computed on HHV or LHV basis, using standard energy balance equations.

2. Heat transfer

- One dimensional steady heat transfer per stage.
- Uniform wall conductivity and thickness, radial conduction only.
- Gas side HTC from standard correlations properties **vary** with temperature pressure and composition.
- Gas radiation via band averaged grey model for CO_2 and H_2O , no spectral resolution, and no soot formation.
- Water side HTC uses IAPWS-IF97 properties, homogenized two phase model.
- Drum at fixed pressure, and perfect steam water separation (no carryover).

3. Hydraulic and thermal performance

- 1D, steady, single phase flow.
- Constant mass flow along each stage.
- Compressibility effects appear only through property variations $\rho(T, P)$ and $\mu(T, P)$ in Re and $\rho V^2/2$.
- Stage level minor loss coefficients are lumped, and uniformly distributed along the stage.
- Gas side ΔP in economizer stage is neglected.

Chapter 4

Combustion Model

Determine combustion conditions inside the furnace (1st pass), resulting in a fully burnt flue gas stream, entering the heat transfer model at adiabatic temperature.

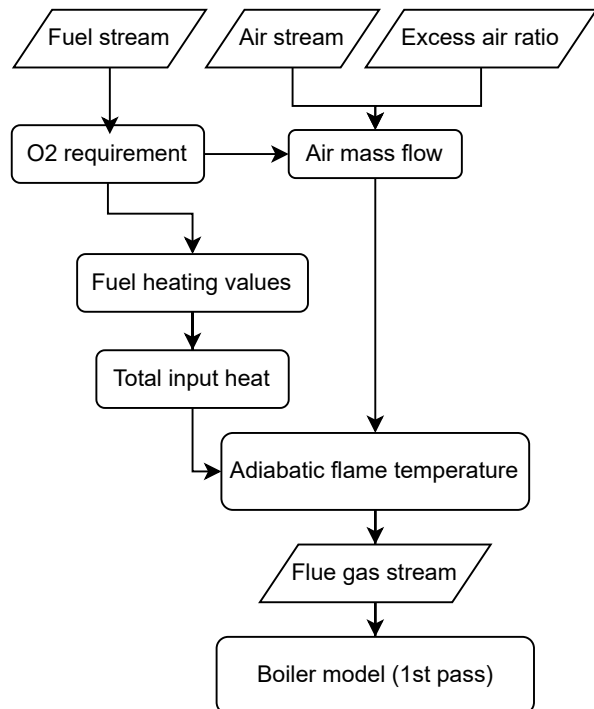


Figure 4.1: Combustion flow

4.1 Fuel and Air

4.1.1 Fuel Stream

The boiler is fired with a natural-gas-type fuel defined in the simulation input (config/fuel.yaml).

The fuel is supplied at $300K$ and $1.013 \times 10^5 Pa$ with a mass flow rate of $0.1kg/s$. Its composition is specified by user on a mass fraction.

Table 4.1: Fuel composition in mass fractions. [1]

Component	Formula	Mass fraction $w_i [-]$
Methane	CH_4	0.8548
Ethane	C_2H_6	0.0622
Propane	C_3H_8	0.0207
n-Butane	C_4H_{10}	0.00518
Hydrogen sulfide	H_2S	0.000104
Nitrogen	N_2	0.0414
Carbon dioxide	CO_2	0.0155
Water vapour	H_2O	0.00
Argon	Ar	0.00

The mass fractions sum to 1.0 by definition. The mole fractions x_i are obtained from

$$x_i = \frac{\frac{w_i}{M_i}}{\sum_j \frac{w_j}{M_j}} \quad (4.1)$$

which is provided by the function `to_mol` in `combustion/mass_mole.py`, where M_i is the molar mass of species i from `molar_masses` in `common/constants.py`.

4.1.2 Air Stream

Combustion air is represented as a separate `GasStream` object, analogous to the fuel stream, with:

- temperature $T_{air} = 300 K$,
- pressure $P_{air} = 1.013 \times 10^5 Pa$,
- mass flow rate determined internally from the specified excess air ratio λ ,
- composition:

Table 4.2: Air composition in mass fractions. [2]

Component	Formula	Mass fraction w_i [-]
Oxygen	O ₂	0.233
Nitrogen	N ₂	0.755
Argon	Ar	0.013
Carbon dioxide	CO ₂	0.00006

The mass fractions satisfy $\sum_i w_i = 1$ and are converted internally to mole fractions whenever stoichiometric or thermophysical properties are required.

4.1.3 Stoichiometric Oxygen requirement

Evaluated the stoichiometric oxygen requirement via `stoich_o2_required_per_mol_fuel` in `combustion/flue.py`. The algorithm is:

1. Use per mole of species stoichiometric O₂ factors $\nu_{O_2,i}$ from `o2_per_mol` in `common/constants.py`:

Table 4.3: Combustion reactions and stoichiometric factors

Species	Global reaction (complete combustion)	$\nu_{O_2,i}$ [mol O ₂ / mol species]
CH ₄	CH ₄ + 2 O ₂ → CO ₂ + 2 H ₂ O	2.0
C ₂ H ₆	C ₂ H ₆ + 3.5 O ₂ → 2 CO ₂ + 3 H ₂ O	3.5
C ₃ H ₈	C ₃ H ₈ + 5 O ₂ → 3 CO ₂ + 4 H ₂ O	5.0
C ₄ H ₁₀	C ₄ H ₁₀ + 6.5 O ₂ → 4 CO ₂ + 5 H ₂ O	6.5
H ₂ S	H ₂ S + 1 O ₂ → SO ₂ + H ₂ O	1.0
N ₂ , CO ₂ , H ₂ O	Inert/fully oxidized → no additional O ₂	0.0

2. Compute the stoichiometric O₂ requirement per mole of fuel mixture as

$$\nu_{O_2,\text{stoich}} = \sum_i x_i \nu_{O_2,i} \quad (4.2)$$

Using the mole fractions from Section 4.1 for the present fuel:

3. For later hydraulic and performance interpretation, it is also useful to express this on a mass basis.

For 1 kg of fuel, the total fuel moles are

$$n_{\text{fuel, total}} = \sum_i \frac{w_i}{M_i} \quad (4.3)$$

Thus the stoichiometric O_2 requirement per unit fuel mass is

$$n_{O_2, \text{stoich}}^{(m)} = \nu_{O_2, \text{stoich}} n_{\text{fuel, total}} \quad (4.4)$$

Converting to mass of O_2 per kg of fuel:

$$\dot{m}_{O_2, \text{stoich}} = n_{O_2, \text{stoich}}^{(m)} M_{O_2} \quad (4.5)$$

For the current working fuel:

- Stoichiometric oxygen requirement: $\nu_{O_2, \text{stoich}} = 2.09$ mol O_2 per mol fuel mixture
- Equivalent mass requirement: $\dot{m}_{O_2, \text{stoich}} = 3.75$ kg O_2 per kg fuel

4.1.4 Air-fuel ratio and excess air λ

The simulation specifies an excess air ratio $\lambda = 1.1$

in config/operation.yaml. This value enters the calculation through air_flow_rates(air, fuel, excess) in combustion/flue.py.

Actual O_2 supplied

Using:

$$\dot{n}_{O_2, \text{actual}} = \lambda \dot{n}_{O_2, \text{stoich}} = \lambda \nu_{O_2, \text{stoich}} \dot{n}_{\text{fuel}} \quad (4.6)$$

Air required

Air O_2 mole fraction (from air.yaml): $x_{O_2, \text{air}} = 0.2095$

Air molar flow, given by air_flow_rates():

$$\dot{n}_{\text{air}} = \frac{\dot{n}_{O_2, \text{actual}}}{x_{O_2, \text{air}}} \quad (4.7)$$

The air molar mass (mixture weighted) is: $M_{\text{air}} = 0.02897$ kg/mol

Therefore the air mass flow rate:

$$\dot{m}_{\text{air}} = \dot{n}_{\text{air}} M_{\text{air}} \quad (4.8)$$

Air-fuel ratio

Mass based air fuel ratio:

$$AFR = \frac{\dot{m}_{air}}{\dot{m}_f} \quad (4.9)$$

4.2 Heating values and firing rate

The fuel lower and higher heating values, and the corresponding firing rate, are evaluated in `combustion/heat.py` by the function `compute_LHV_HHV(fuel)` and then used by `total_input_heat()`.

4.2.1 HHV and LHV

For each fuel species, complete combustion is considered:

- $CH_4 + 2 O_2 \rightarrow CO_2 + 2 H_2O$
- $C_2H_6 + 3.5 O_2 \rightarrow 2 CO_2 + 3 H_2O$

Builds product formation enthalpies for:

- HHV assumption: water as liquid (condensed)
- LHV assumption: water as vapour (no condensation heat recovered)

Latent heat of water

Obtain the latent heat of vaporization of water at the reference pressure $P_{ref} = 101,325 \text{ Pa}$ from the IAPWS-97 correlation:

```
latent_H2O = WaterProps.h_g(P_ref) - WaterProps.h_f(P_ref)
```

where:

- h_g is the saturated vapour enthalpy,
- h_f is the saturated liquid enthalpy.

Reference formation enthalpies

Standard formation enthalpies Δh_f° (at 298.15 K, 1 bar) are taken from `common/constants.py` in kJ/mol:

Table 4.4: Standard enthalpy of formation of selected species [3]

Species	Δh_f° (kJ mol $^{-1}$)
CH ₄	-74.8
C ₂ H ₆	-84.7
C ₃ H ₈	-103.8
C ₄ H ₁₀	-126.1
SO ₂	-296.8
CO ₂	-393.5
H ₂ O(l)	-285.5

Methodology

The mixture molar higher and lower heating values are:

$$\text{HHV}_{\text{mol}} = h_{\text{react}} - h_{\text{prod,HHV}}, \quad \text{LHV}_{\text{mol}} = h_{\text{react}} - h_{\text{prod,LHV}} \quad (4.10)$$

These are converted to mass based heating values.

For each species i in the fuel, the reaction enthalpy contribution is

$$\Delta h_i = x_i [\Delta h_{f,\text{products}}^\circ - \Delta h_{f,\text{reactants}}^\circ], \quad (4.11)$$

and mixture HHV and LHV are obtained by summing these contributions over all fuel components, enforcing the appropriate water phase:

- HHV: water in products is liquid
- LHV: water in products is vapour

After obtaining the mixture molar heating values, conversion to mass basis uses

$$\text{HHV}_{\text{mix}} = \frac{\text{HHV}_{\text{mol}}}{M_{\text{mix}}}, \quad \text{LHV}_{\text{mix}} = \frac{\text{LHV}_{\text{mol}}}{M_{\text{mix}}}, \quad (4.12)$$

The firing rate corresponding to a fuel mass flow \dot{m}_f then follows directly:

$$P_{\text{HHV}} = \dot{m}_f \text{HHV}_{\text{mix}}, \quad P_{\text{LHV}} = \dot{m}_f \text{LHV}_{\text{mix}}. \quad (4.13)$$

For the fuel specified above, the mixture heating values are:

Table 4.5: Heating values and firing rates, returned by `compute_LHV_HHV()`

Variable	Value
HHV_{mix}	52 MJ/kg
LHV_{mix}	47 MJ/kg
P_{HHV}	26 MW
P_{LHV}	23.6 MW

4.2.2 Total heat input

The function `total_input_heat()` combines chemical and sensible contributions:

where `sensible_heat()` uses:

$$Q_{\text{sens}} = \dot{m} c_p (T - T_{\text{ref}}) \quad (4.14)$$

Both fuel and air enter at 300 K, while the reference is 298.15 K; the resulting sensible contributions are very small compared with the chemical term P_{LHV} (on the order of tens of kW versus tens of MW). Therefore:

$$Q_{\text{in}} = P_{\text{LHV}} + Q_{\text{sens,fuel}} + Q_{\text{sens,air}} \quad (4.15)$$

4.3 Adiabatic flame temperature

The adiabatic flame temperature T_{ad} is evaluated in the model by the function `adiabatic_flame_T()` in `combustion/adiabatic_flame_temperature.py`. This routine uses Cantera and an enthalpy–pressure equilibrium (HP) function to determine the equilibrium temperature and composition of the flue gas, assuming:

- complete mixing of fuel and air,
- no heat losses to the surroundings (adiabatic),
- constant system pressure (equal to the air/fuel inlet pressure),
- chemical equilibrium among all gas species.

The total inlet enthalpy rate of the unmixed reactants is

$$\dot{H}_{\text{react}} = \dot{m}_{\text{air}} h_{\text{air}}(T_{\text{air}}, P, X_{\text{air}}) + \dot{m}_{\text{fuel}} h_{\text{fuel}}(T_{\text{fuel}}, P, X_{\text{fuel}}) \quad (4.16)$$

The total mass flow is

$$\dot{m}_{\text{tot}} = \dot{m}_{\text{air}} + \dot{m}_{\text{fuel}} \quad (4.17)$$

so the mixture-averaged specific enthalpy of the reactants is

$$h_{\text{target}} = \frac{\dot{H}_{\text{react}}}{\dot{m}_{\text{tot}}} \quad (4.18)$$

The adiabatic, constant-pressure equilibrium state is then defined by the constraints:

$$\begin{aligned} h_{\text{products}}(T_{\text{ad}}, P, \mathbf{X}_{\text{eq}}) &= h_{\text{target}} \\ P_{\text{out}} &= P \\ \mathbf{X}_{\text{eq}} &\text{satisfies chemical equilibrium at } (T_{\text{ad}}, P) \end{aligned} \quad (4.19)$$

Cantera is used to enforce this condition via its HP equilibrium mode.

Build the overall reactant composition $\mathbf{X}_{\text{react}}$ from the molar flow rates of each component in each stream:

Determine molar flow rates of all species in the air and fuel streams,

$$\dot{n}_i^{(\text{air})}, \quad \dot{n}_i^{(\text{fuel})}. \quad (4.20)$$

Form the total species molar flow rate,

$$\dot{n}_i = \dot{n}_i^{(\text{air})} + \dot{n}_i^{(\text{fuel})}. \quad (4.21)$$

Compute the overall reactant mole fractions,

$$X_{i,\text{react}} = \frac{\dot{n}_i}{\sum_j \dot{n}_j} \quad (4.22)$$

Initialize the mixture and perform HP equilibrium:

Initialize the reacting mixture at temperature $T = 300$ K, pressure P , and composition X_{react} .

Impose the constraint of fixed enthalpy and pressure,

$$h = h_{\text{target}}, \quad P = P, \quad (4.23)$$

and compute the chemical equilibrium state under (H, P) conditions.

Obtain the equilibrium mass fractions

$$Y_{i,\text{eq}} \quad (4.24)$$

The HP-equilibrium calculation yields an adiabatic flame temperature on the order of:

$$T_{\text{ad}} = 2,050 \text{ K} \quad (= 1,780^\circ\text{C}) \quad (4.25)$$

This value is consistent with typical adiabatic flame temperatures for natural gas with around 10 % excess air and confirms that the combustion zone (furnace) operates at very high gas temperatures [4], driving strong radiative and convective heat transfer to the shell-side water/steam.

4.4 Flue gas composition

In the combustion model two different flue gas streams are distinguished, represented as `GasStream` objects and stored in the `CombustionResult`, but they serve different purposes in the boiler calculation:

1. Equilibrium flue gas (`f1ue_ad`)

- Defined as the flue gas mixture at adiabatic flame conditions, obtained from a high-temperature HP equilibrium calculation in Cantera.
- Contains all equilibrium species permitted by the reaction mechanism.
- Its purposes are:
 - determining the adiabatic flame temperature T_{ad} ,
 - providing the equilibrium composition for diagnostics.

2. Fully burnt flue gas (`f1ue`)

- Defined as a chemically frozen, fully burnt mixture at the same temperature and pressure as the equilibrium (`f1ue_ad`).
- Contains only standard engineering combustion products.
- Used as the hot side working gas for all boiler heat transfer and pressure drop calculations throughout the heat-exchanger network.

The equilibrium flue gas provides a physically consistent high temperature reference, while the fully burnt flue gas represents the practical working fluid in the convective radiative sections of the boiler.

Fully burnt boiler flue gas

Starting from the fuel and air known `GasStream` objects, compute molar formation rates and flow rate as:

Using the fuel and air molar flow rates, \dot{n}_{fuel} and \dot{n}_{air} , and their mole fractions $x_i^{(\text{fuel})}$ and $x_i^{(\text{air})}$, for any product species k , the molar flow rate is written generically as

$$\dot{n}_k = \dot{n}_{\text{fuel}} \Phi_k^{(\text{fuel})} + \dot{n}_{\text{air}} \Phi_k^{(\text{air})}, \quad (4.26)$$

where

- $\Phi_k^{(\text{fuel})}$ is the amount of species k that comes from the fuel: species already present in the fuel plus any of k formed by complete oxidation of the fuel components.
- $\Phi_k^{(\text{air})}$ is the amount of species k that comes from the air: species originally present in the air plus any portion that remains unreacted.

Oxygen additionally satisfies

$$\dot{n}_{O_2} = \dot{n}_{\text{air}} x_{O_2}^{(\text{air})} - \dot{n}_{\text{fuel}} \nu_{O_2, \text{stoich}}, \quad (4.27)$$

where $\nu_{O_2, \text{stoich}}$ is the stoichiometric oxygen demand of the fuel.

The total molar flow rate of the fully burnt flue gas is

$$\dot{n}_{\text{tot}} = \sum_k \dot{n}_k. \quad (4.28)$$

The molar fractions of the products are then

$$x_k^{(\text{flue})} = \frac{\dot{n}_k}{\dot{n}_{\text{tot}}}. \quad (4.29)$$

These molar fractions are converted to product mass fractions by `to_mass()`:

$$w_k^{(\text{flue})} = \frac{x_k^{(\text{flue})} M_k}{\sum_j x_j^{(\text{flue})} M_j}. \quad (4.30)$$

Finally, the flue gas total mass flow rate is obtained from the molar composition and total molar flow via `mass_flow()`:

$$\dot{m}_{\text{flue}} = \sum_k x_k^{(\text{flue})} \dot{n}_{\text{tot}} M_k. \quad (4.31)$$

The function `from_fuel_and_air()` returns the fully burnt flue gas composition $w_k^{(\text{flue})}$ and the total flue mass flow \dot{m}_{flue} .

This separation allows the model to retain a realistic high temperature reference from chemical equilibrium while employing a reduced, engineering flue gas composition for subsequent heat transfer and hydraulic calculations.

Chapter 5

Heat Transfer Model

This model simulates heat transfer from hot flue gas to the water/steam mixture in the drum, flue gas entering first pass, is specified by the results of the combustion model as fully burnt gas at adiabatic temperature with known mass flow rate, and water entering the economizer, specified by user at 10bar pressure and 105°C temperature with the mass flow to be calculated iteratively until convergence of water in and steam produced.

5.1 Fundamental heat balance equations

The boiler is modelled as a one dimensional counter current heat exchanger composed of six stages (HX_1-HX_5). Heat transfer is resolved along the gas flow direction x , while water flows in the opposite direction. Each stage is discretized into segments of length dx ; all local quantities are defined per unit length.

- Notation (per segment)
- x – axial coordinate along the gas flow [m]
- dx – marching step in x [m]
- \dot{m}_g, \dot{m}_w – gas and water mass flow rates [kg/s]
- $T_g(x), T_w(x)$ – bulk gas and water temperatures [K]
- $T_{gw}(x), T_{ww}(x)$ – gas-side and water-side wall temperatures [K]
- $h_g(x), h_w(x)$ – total gas-side and water-side heat-transfer coefficients [$W/m^2 \cdot K$]
- P_g, P_w – gas-side and water-side wetted perimeters [m]
- $q'(x)$ – linear heat flux (heat per unit length) [W/m]
- $UA'(x)$ – overall conductance per unit length [$W/K/m$]

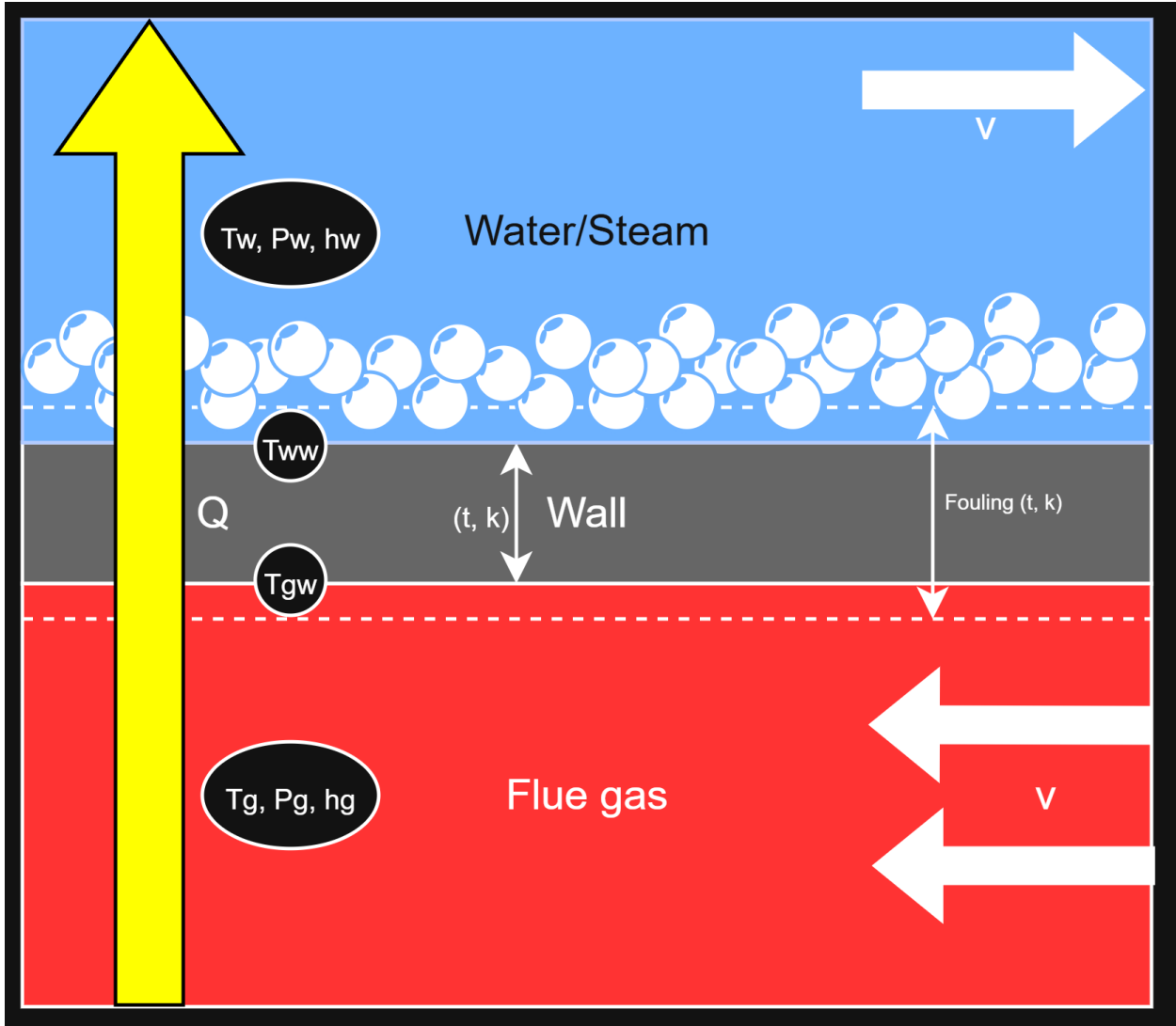


Figure 5.1: Cross section of heat transfer network from gas to water/steam

5.2 Local energy balance

For each differential segment of length dx , the model enforces a one dimensional steady state energy balance between the gas, the water and the tube wall:

- Heat transferred across the wall:

$$q'(x) = UA'(x) [T_g(x) - T_w(x)] \quad (5.1)$$

- Relation to the segment duty:

$$dQ(x) = q'(x) dx \quad (5.2)$$

- Gas stream:

$$dQ(x) = -\dot{m}_g dh_g(x) \Rightarrow \frac{dh_g}{dx} = -\frac{q'(x)}{\dot{m}_g} \quad (5.3)$$

- Water stream:

$$dQ(x) = +\dot{m}_w dh_w(x) \Rightarrow \frac{dh_w}{dx} = +\frac{q'(x)}{\dot{m}_w} \quad (5.4)$$

In the numerical implementation these equations are applied in finite difference form over each marching step:

$$Q_{\text{step}} = q'(x) \Delta x \quad (5.5)$$

$$\Delta h_g = -\frac{Q_{\text{step}}}{\dot{m}_g}, \quad \Delta h_w = +\frac{Q_{\text{step}}}{\dot{m}_w} \quad (5.6)$$

5.3 Overall conductance and resistance network

The overall conductance per unit length $UA'(x)$ is obtained from a radial series of thermal resistances per unit length:

- Gas side convection:

$$R'_g = \frac{1}{h_g(x) P_g} \quad (5.7)$$

- Gas side fouling:

$$R'_{fg} = R'_{fi}(P_g) \quad (\text{from specified fouling thickness and conductivity}) \quad (5.8)$$

- Tube wall:

$$R'_w = \frac{\ln(D_o/D_i)}{2\pi k_w} \quad (5.9)$$

- Water side fouling:

$$R'_{fc} = R'_{fo}(P_w) \quad (5.10)$$

- Water side convection:

$$R'_c = \frac{1}{h_w(x) P_w} \quad (5.11)$$

where D_i and D_o are the tube inner and outer diameters and k_w is the tube wall thermal conductivity. Combining these contributions:

$$\frac{1}{UA'(x)} = R'_g + R'_{fg} + R'_w + R'_{fc} + R'_c \quad (5.12)$$

or equivalently,

$$UA'(x) = \left[\frac{1}{h_g P_g} + R'_{fg} + R'_w + R'_{fc} + \frac{1}{h_w P_w} \right]^{-1} \quad (5.13)$$

The linear heat flux then follows directly:

$$q'(x) = UA'(x) [T_g(x) - T_w(x)] \quad (5.14)$$

5.4 Wall temperature update and thermal convergence

The tube wall temperatures on the gas and water sides, T_{gw} and T_{ww} , are updated using a two node wall model in each marching step.

Given $q'(x)$, the wall side energy balances yield:

$$T_{gw} = T_g - \frac{q'}{h_{g,\text{tot}}} \quad (5.15)$$

$$T_{ww} = T_w + \frac{q'}{h_w} \quad (5.16)$$

The wall conduction temperature drop is:

$$\Delta T_{\text{wall}} = T_{gw} - T_{ww} \quad (5.17)$$

which is also equal to:

$$\Delta T_{\text{wall}} = q' [R'_{fg} + R'_w + R'_{fc}] \quad (5.18)$$

A consistency check is applied; if the implied wall temperature difference from conduction differs from the one implied by convection, the marching solver iterates the HTC evaluation once with relaxed updates (default under-relaxation factor 0.35).

In the actual implementation this consistency check is performed by iterating on T_{gw} , T_{ww} , and q' using the full resistance network (gas convection, gas fouling, wall, water fouling, water convection), with an under-relaxation factor applied to both wall temperatures and the linear heat flux.

If temperature overshoot (negative film coefficient, reversed driving force) is detected within a step, the step is automatically halved and recomputed.

5.5 Stage and boiler level duties

For a stage of length L_j , the stage heat duty and stage level conductance are obtained by integrating the local quantities along x :

$$Q_{\text{stage},j} = \int_0^{L_j} q'(x) \, dx \approx \sum_i q'_i \Delta x_i \quad (5.19)$$

$$(UA)_j = \int_0^{L_j} UA'(x) \, dx \approx \sum_i UA'_i \Delta x_i \quad (5.20)$$

The total useful boiler duty is the sum of all stage duties:

$$Q_{\text{useful}} = \sum_{j=1}^6 Q_{\text{stage},j} \quad (5.21)$$

These integrated quantities are later used in the performance and efficiency evaluation (Section 7) and for constructing stage-wise summary tables.

T-Q diagram of a typical 3 pass shell boiler

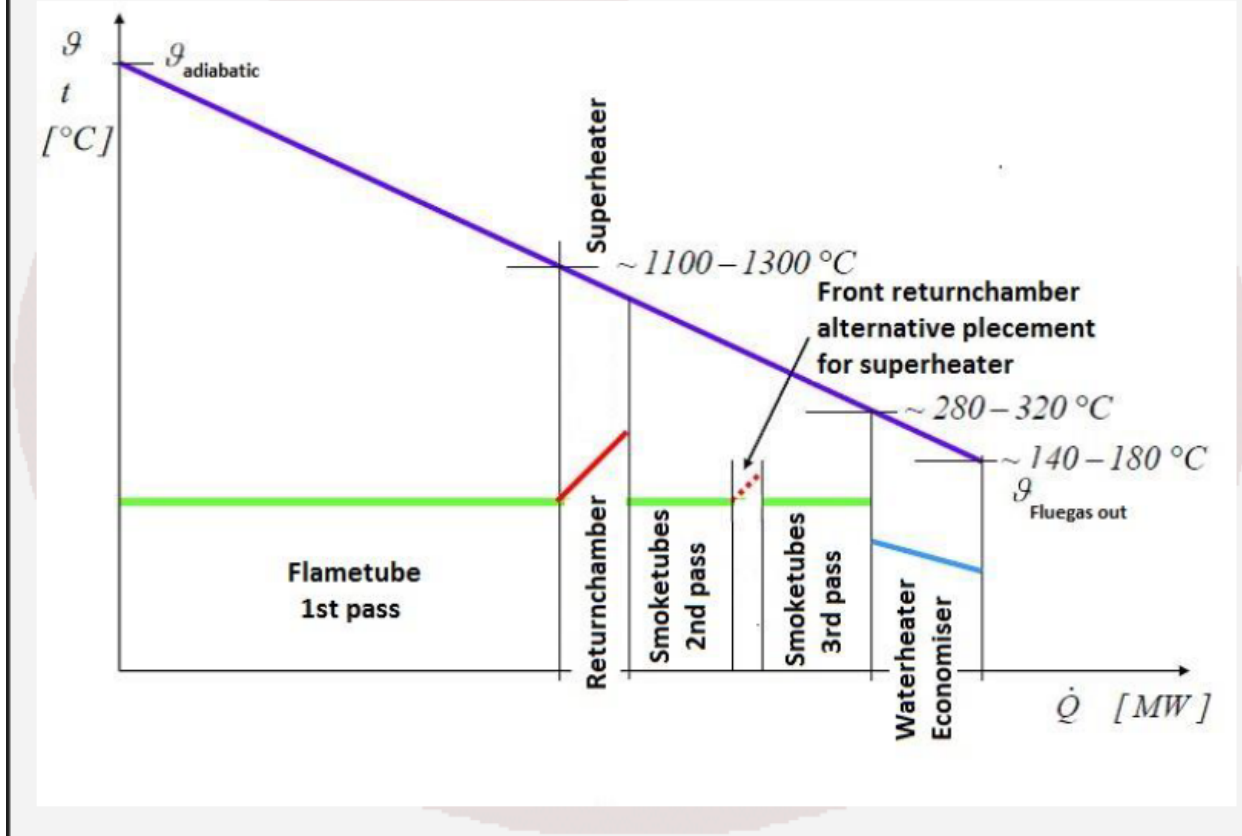


Figure 5.2: Representative T - Q diagram for the three pass boiler, showing gas and water/steam temperature evolution and stage heat duties $HX_1 - HX_6$.

5.6 Gas side

Gas side heat transfer is computed with geometry aware correlations based on local gas properties from Cantera (GasProps) and stage specific geometry from the GeometryBuilder. For each marching step, the total gas side HTC is split into a convective and a radiative contribution:

$$h_{g,\text{tot}} = h_{g,\text{conv}} + h_{g,\text{rad}} \quad (5.22)$$

The implementation uses the helper `gas_htc_parts(g, spec, T_{gw})`, which returns $(h_{g,\text{conv}}, h_{g,\text{rad}})$ in $\text{W/m}^2\cdot\text{K}$, and then sums them in `gas_htc`.

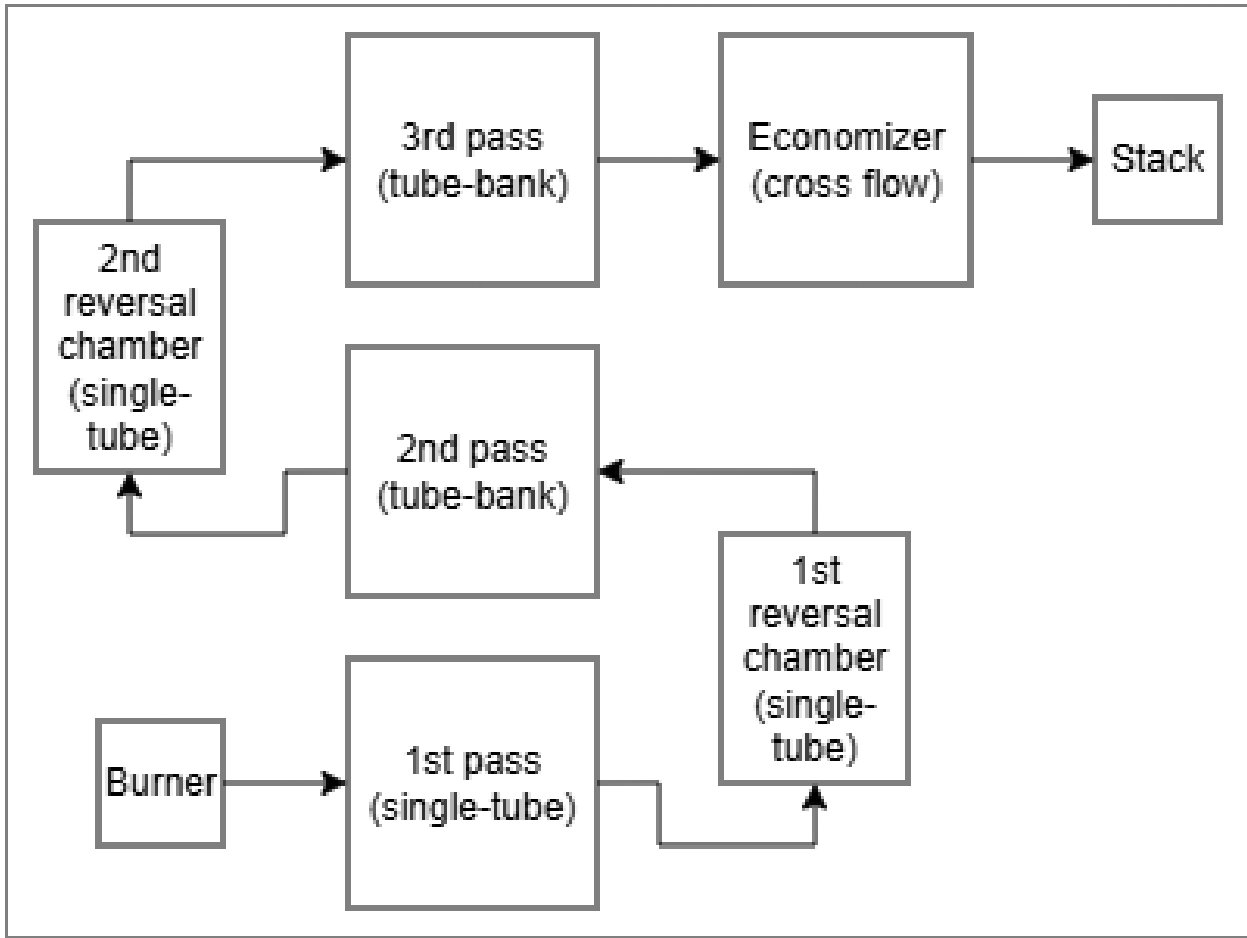


Figure 5.3: Path of flue gas through the 6 stages

5.6.1 Single tube and reversal chamber

Stages of kind `single_tube` and `reversal_chamber`, corresponding to furnace (first pass), and both reversal chambers, are treated as internal forced convection in a circular duct. The characteristic quantities are:

- Diameter: D (supplied by `stages.yaml`)
- Length: L (supplied by `stages.yaml`)
- Flow area: $A = \frac{1}{4} \pi D^2$ (calculated by geometry builder)
- Velocity:

$$V = \frac{\dot{m}_g}{\rho_g A} \quad (5.23)$$

- Reynolds and Prandtl numbers:

$$\text{Re} = \frac{\rho_g V D}{\mu_g}, \quad \text{Pr} = \frac{c_{p,g} \mu_g}{k_g} \quad (5.24)$$

Local gas properties $\rho_g, \mu_g, k_g, c_{p,g}$ are obtained from the Cantera mixture via the functions defined in `common\props.py`, at the local gas temperature and pressure. [5]

Laminar/developing flow (Graetz-type)

For $Re < 2300$, uses a Graetz correlation for thermally developing laminar flow:

$$Gz = Re \Pr \frac{D}{L} \quad (5.25)$$

$$Nu = 3.66 + \frac{0.0668 Gz}{1 + 0.04 Gz^{2/3}} \quad (5.26)$$

[6]

Turbulent flow (Gnielinski with Petukhov friction factor)

For $Re \geq 2300$, the Gnielinski correlation is applied with a Petukhov friction factor:

$$f = (0.79 \ln Re - 1.64)^{-2} \quad (5.27)$$

[7]

$$Nu = \frac{\frac{f}{8}(Re - 1000) \Pr}{1 + 12.7 \sqrt{\frac{f}{8}} (\Pr^{2/3} - 1)} \quad (5.28)$$

[6] The local convective heat-transfer coefficient is then:

$$h_{g,\text{conv}} = \frac{Nu k_g}{D} \quad (5.29)$$

[6]

This same internal correlation is used for `single_tube`, `reversal_chamber` and `tube_bank` gas-side flow (see below).

5.6.2 Tube bank

Stages `tube_bank` correspond to tube bundles inside the shell, ie. first and second passes. In this model, the gas side is still treated as internal flow inside the tubes:

- Hot side (gas): inside tubes (inner diameter D_i), using the same internal forced convection model as in Section 5.2.1.

Thus the gas side convective HTC in tube-bank stages is:

$$h_{g,\text{conv}}^{(\text{HX3,5})} = \frac{\text{Nu}(\text{Re}, \text{Pr}) k_g}{D_i} \quad (5.30)$$

with Nu given by the Graetz/Gnielinski formulation above, and Re, Pr computed from the local gas properties and tube hydraulic diameter.

5.6.3 Economizer

The economizer stage reverses the roles: gas flows outside the tubes in cross flow, while water flows inside. The gas side convection is then modelled as external cross flow over a tube bank.

Key geometry quantities (from `GeometryBuilder` for the economizer):

- Tube outer diameter: $D = D_o$
- Gas side cross flow area: $A_{\text{bulk}} = A_{\text{hot,flow}}$
- Optional maximum/mean velocity factor:

$$V_{\text{bulk}} = \frac{\dot{m}_g}{\rho_g A_{\text{bulk}}}, \quad V = u_{\text{max}} V_{\text{bulk}} \quad (5.31)$$

where u_{max} is calculated depending on the tube bank arrangement and spacing between tubes.

- Reynolds and Prandtl numbers:

$$\text{Re} = \frac{\rho_g V D}{\mu_g}, \quad \text{Pr} = \frac{c_{p,g} \mu_g}{k_g} \quad (5.32)$$

For "economiser" stages the primary correlation is a banded Zukauskas form for cross flow over tube banks:

$$\text{Nu} = C \text{Re}^m \text{Pr}^n \quad (5.33)$$

[6]

where the coefficients C, m are selected from standard bands as a function of Reynolds number and tube arrangement (inline vs staggered), and the exponent n is:

$$n = \begin{cases} 0.36, & \text{Pr} \leq 10 \\ 0.25, & \text{Pr} > 10 \end{cases} \quad (5.34)$$

If Re falls outside the tabulated bands, the model falls back to the Churchill–Bernstein correlation for cross flow over a single cylinder:

$$\text{Nu} = 0.3 + \frac{0.62 \text{Re}^{1/2} \text{Pr}^{1/3}}{\left[1 + (0.4/\text{Pr})^{2/3}\right]^{1/4}} \left[1 + \left(\frac{\text{Re}}{282000}\right)^{5/8}\right]^{4/5} \quad (5.35)$$

[6] The gas-side convective HTC in the economizer is then:

$$h_{g,\text{conv}}^{(\text{HX6})} = \frac{\text{Nu } k_g}{D_o} \quad (5.36)$$

[6]

5.6.4 Radiation model

Radiative heat transfer from the flue gas to the furnace surfaces is explicitly accounted for by a participating medium model for the H_2O/CO_2 mixture. The implementation follows a simplified Smith–Shen–Friedman style four gray model.

For each step, the gas emissivity is computed as:

1. Partial pressures of participating species:

$$p_{H_2O} = y_{H_2O} P, \quad p_{CO_2} = y_{CO_2} P \quad (5.37)$$

[8] where y_i are molar (or mass-fraction-equivalent) composition entries from the flue gas stream, and P is the local gas pressure.

2. Mean beam length:

$$L_b = \begin{cases} L_{\text{rad,override}}, & \text{if specified in the stage} \\ 0.9 D_{h,\text{gas}}, & \text{otherwise} \end{cases} \quad (5.38)$$

[8] with $D_{h,\text{gas}}$ the gas-side hydraulic diameter.

3. Effective optical thickness in each gray band:

$$p_{\text{ratio}} = \frac{p_{H_2O} + p_{CO_2}}{P_{\text{atm}}} \quad (5.39)$$

[8]

$$\tau_j = K_j \left(\frac{T}{1000 \text{ K}} \right)^{T_{\text{exp}}} p_{\text{ratio}} L_b \quad (5.40)$$

[8]

where K_j and weighting factors A_j are fixed band coefficients, T is the gas temperature, and T_{exp} is a temperature exponent (default 0.65, configurable per stage via `rad_Texp`).

4. Total gas emissivity:

$$\varepsilon_g = 1 - \sum_{j=1}^4 A_j \exp(-\tau_j) \quad (5.41)$$

[8] with ε_g constrained to $[0, 1]$.

A mean-film temperature is used for the linearized radiative HTC:

$$T_{\text{film}} = \frac{T_g + T_{gw}}{2} \quad (5.42)$$

$$h_{g,\text{rad}} = 4 \sigma F \varepsilon_g T_{\text{film}}^3 \quad (5.43)$$

[8]

where:

- σ is the Stefan–Boltzmann constant,
- F is an effective view factor (default 1.0 or stage-specific `rad_F`).

The gas-side total HTC reported and used in the resistance network is then:

$$h_{g,\text{tot}} = h_{g,\text{conv}} + h_{g,\text{rad}} \quad (5.44)$$

and the corresponding convective/radiative contributions to the linear heat flux are tracked via:

$$q'_{\text{conv}} = q' \frac{h_{g,\text{conv}}}{h_{g,\text{tot}}}, \quad q'_{\text{rad}} = q' - q'_{\text{conv}} \quad (5.45)$$

These diagnostics are later integrated on a per-stage basis to quantify the share of convective vs radiative heat transfer in each section of the boiler.

5.7 Water side

Water side heat transfer is computed with geometry dependent correlations using local water properties from IAPWS97 (WaterProps), with stage specific geometry from the GeometryBuilder. The solver always works with a single effective water side heat transfer coefficient $h_w(x)$ per marching step, which may represent:

- pure pool boiling at a saturated surface,
- a Chen type combination of forced convection and nucleate boiling, or
- single phase forced convection.

In the implementation this logic is encapsulated in `water_htc`, which returns (h_w) for each step.

5.7.1 General formulation and boiling treatment

The six stages of the boiler are divided, from the water-side point of view, into:

- HX_1-HX_5 : pool-boiling stages
(`pool_boiling = true` in the stage specification)
- HX_6 : economizer stage
(`pool_boiling = false`)

Process in boilers drawn in T-S chart

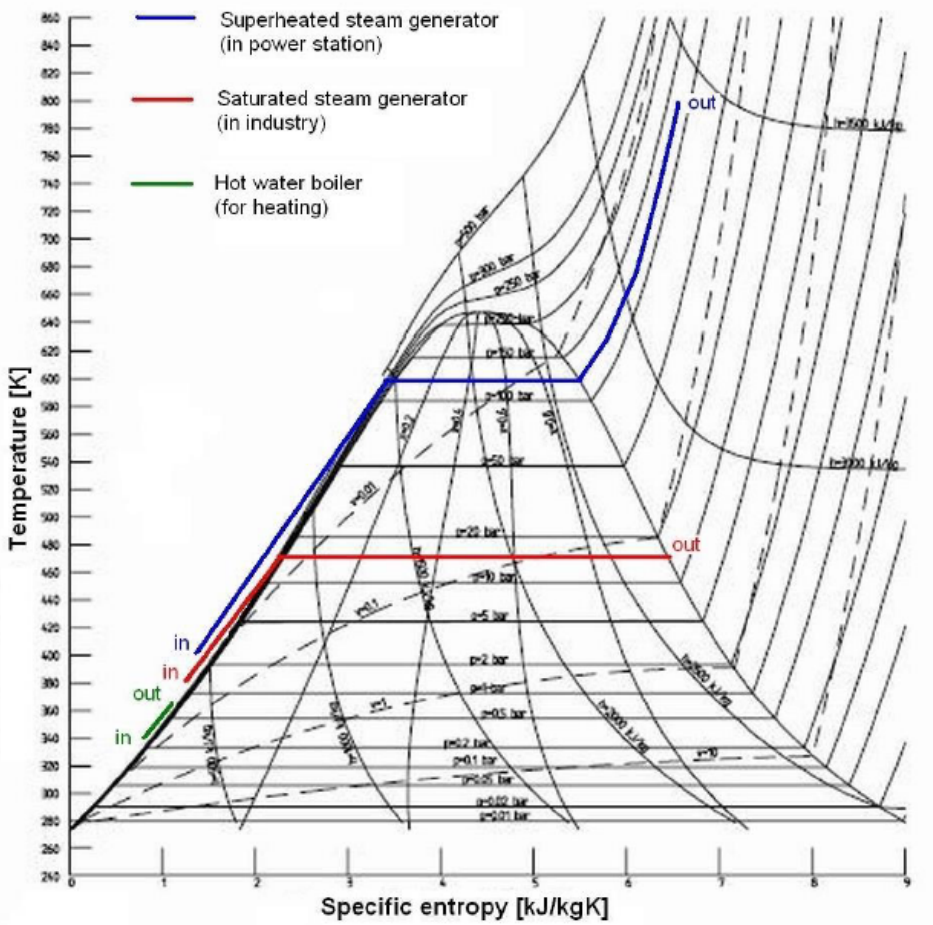


Figure 5.4: Temperature–entropy (T – s) representation of the feedwater heating and evaporation process across economiser and boiler at the operating pressure.

The solver applies the following decision tree at each marching step:

1. Pool-boiling stages (HX_1 – HX_5)

If the stage is flagged as `pool_boiling = true`, the bulk water temperature entering the wall-energy balance is fixed at the saturation temperature at the local pressure:

$$T_w = T_{\text{sat}}(p_w), \quad (5.46)$$

and the water-side HTC is computed from the Cooper pool boiling correlation for nucleate boiling correlation:

$$h_{\text{Cooper}} = 55 p_r^{0.12} R_p^{-0.55} M_w^{-0.5} (q'')^{0.67} \quad (5.47)$$

where

$$p_r = \frac{p}{p_{\text{crit}}} = \text{reduced pressure}, \quad R_p = \text{surface roughness } (\mu\text{m}), \quad q'' = \text{heat flux}. \quad (5.48)$$

[6]

This nucleate-boiling HTC is then used directly:

$$h_w = h_{w,\text{nb}}, \quad (5.49)$$

and the step is always marked as boiling in the post processing.

In other words, the main boiling surfaces of the boiler (furnace, passes, reversal chambers) are represented as heated surfaces in a saturated pool, with the HTC governed by the local heat flux and surface roughness rather than by a detailed prediction of liquid velocity. This matches the natural circulation character of these sections.

2. Non pool boiling stages (HX₆, economizer)

For stages with `pool_boiling = false`, the model can represent both single phase convection and flow boiling via a Chen type formulation.

a. Boiling detection

A helper determines whether the local state is boiling based on the bulk enthalpy h and, when needed, the wall temperature T_{wall} :

- if

$$h_f(p_w) \leq h \leq h_g(p_w) \quad (5.50)$$

the state is inside the saturation interval and is treated as two phase;

- if $h < h_f(p_w)$ (slightly subcooled liquid) but the wall superheat is sufficiently high,

$$T_{\text{wall}} > T_{\text{sat}}(p_w) + \Delta T_{\text{crit}}, \quad (5.51)$$

the state is also treated as boiling;

- otherwise the flow is treated as single-phase liquid.

Here h_f and h_g are saturated-liquid and saturated vapor enthalpies at the local pressure, obtained via IAPWS97.

b. Single-phase regime

If boiling is not detected, the water side HTC is purely convective:

$$h_w = h_{w,\text{conv}}, \quad (5.52)$$

with $h_{w,\text{conv}}$ obtained from a geometry dependent forced convection correlation (internal tube, external tube bank, or external single tube/bend) as detailed in Sections [5.7.2]–[5.7.4].

c. Flow boiling regime (Chen model)

When boiling is detected in a non pool boiling stage, the HTC is constructed as a Chen type superposition of:

- a liquid only convective term h_{lo} , and
- a nucleate-boiling term h_{nb} using the same Cooper correlation as in pool boiling.

The liquid only HTC is evaluated at the saturation temperature $T_{\text{sat}}(p)$ and using the appropriate geometry correlation:

$$h_{\text{lo}} = h_{\text{single-phase}}(T_{\text{sat}}(p), \text{geometry}), \quad (5.53)$$

while the nucleate-boiling term is

$$h_{\text{nb}} = h_{\text{Cooper}}(p, q''). \quad (5.54)$$

The Chen combination used in the code is:

$$h_w = F h_{\text{lo}} + S h_{\text{nb}}. \quad (5.55)$$

[6]

The convection enhancement factor F is based on a Martinelli type parameter X_{tt} ,

$$X_{tt} = \left(\frac{1-x}{x}\right)^{0.9} \left(\frac{\mu_l}{\mu_g}\right)^{0.1} \left(\frac{\rho_g}{\rho_l}\right)^{0.5}, \quad (5.56)$$

where x is the local vapor quality and $\rho_l, \rho_g, \mu_l, \mu_g$ are liquid/vapor densities and viscosities at saturation. A bounded form of the Chen factor is then used:

$$F = 1 + 0.12 X_{tt}^{-0.8}, \quad (5.57)$$

The suppression factor S modulating the nucleate boiling contribution is a function of mass flux and Reynolds number:

$$S = \frac{1}{1 + C \text{Re}_{\text{lo}}^\alpha}, \quad (5.58)$$

where Re_{lo} is a liquid only Reynolds number based on the mass flux

$$G = \frac{\dot{m}_w}{A_{\text{flow}}}, \quad (5.59)$$

and the liquid properties at saturation. In the implementation the constants and bounds are chosen such that S remains between about 0.1 and 1.0, reducing the nucleate boiling influence at very high mass flux (strong forced convection).

In the present thesis this Chen type flow boiling capability is only exercised in the economizer stage; the main boiling sections (HX_1 – HX_5) use the pure pool boiling representation above.

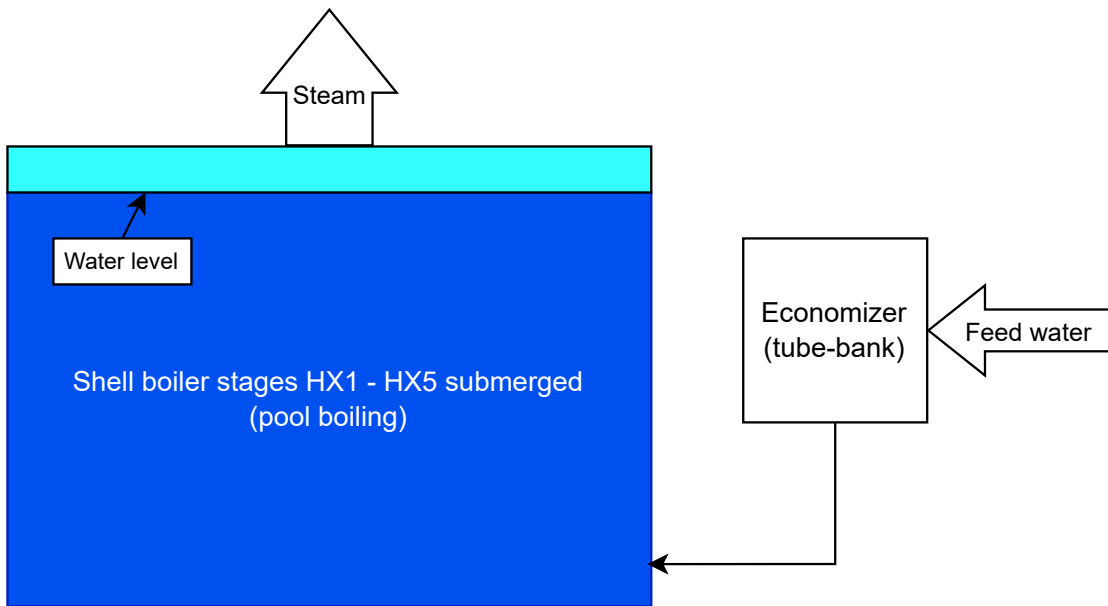


Figure 5.5: Path of water/steam through the 6 stages

5.7.2 Economizer

In the economizer stage (HX_6 , kind = "economiser"), water flows inside the tubes and is heated by the flue gas flowing externally in cross flow. This stage is the only one where `pool_boiling = false` and where the full single phase/Chen type boiling formulation is used.

Velocity and dimensionless groups

The relevant geometric quantities for the water side are:

- tube inner diameter: D_i ,
- tube length: L ,

- cold-side flow area: $A_{\text{cold,flow}}$.

The bulk water velocity, Reynolds and Prandtl numbers are:

$$V_w = \frac{\dot{m}_w}{\rho_w A_{\text{cold,flow}}}, \quad (5.60)$$

$$\text{Re}_w = \frac{\rho_w V_w D_i}{\mu_w}, \quad \text{Pr}_w = \frac{c_{p,w} \mu_w}{k_w}, \quad (5.61)$$

with $\rho_w, \mu_w, k_w, c_{p,w}$ evaluated from IAPWS97 at the film temperature. [9]

Single phase internal flow correlation

When no boiling is detected in the economizer, the Nusselt number is computed using a Gnielinski type internal flow correlation with a viscosity ratio correction:

- Laminar / developing regime ($\text{Re}_w < 2300$): a Graetz type form is used

$$\text{Gz}_w = \text{Re}_w \text{Pr}_w \frac{D_i}{L}, \quad (5.62)$$

$$\text{Nu}_w = 3.66 + \frac{0.0668 \text{Gz}_w}{1 + 0.04 \text{Gz}_w^{2/3}}. \quad (5.63)$$

- Turbulent regime ($\text{Re}_w \geq 2300$): Gnielinski correlation with friction factor

$$f_w = (0.79 \ln \text{Re}_w - 1.64)^{-2}, \quad (5.64)$$

[7]

$$\text{Nu}_w = \frac{\frac{f_w}{8} (\text{Re}_w - 1000) \text{Pr}_w}{1 + 12.7 \sqrt{\frac{f_w}{8}} (\text{Pr}_w^{2/3} - 1)}, \quad (5.65)$$

[6] scaled by a viscosity-ratio correction:

$$\text{Nu}_w \leftarrow \text{Nu}_w \left(\frac{\mu_b}{\mu_w} \right)^{0.11}, \quad (5.66)$$

where μ_b is evaluated at the bulk temperature and μ_w at the wall temperature.

The single phase water side HTC in the economizer is then:

$$h_{w,\text{conv}}^{(\text{HX6})} = \frac{\text{Nu}_w k_w}{D_i}. \quad (5.67)$$

[6]

Flow boiling in the economizer

If boiling is detected in the economizer (according to the criteria in the general formulation), the same geometry and mass flux information are used to form the liquid only HTC h_{lo} and the Cooper nucleate boiling HTC h_{nb} . The total water side HTC is then:

$$h_w = F h_{lo} + S h_{nb}, \quad (5.68)$$

with F and S given by the Chen type relations described above, using the local vapor quality, mass flux, and saturation properties. This provides a smooth transition between predominantly convective and predominantly nucleate boiling regimes in the economizer.

5.7.3 Tube bank stages

For completeness, the water side model also includes correlations for cross flow over tube banks on the cold side (`kind = "tube_bank"`), although in the present thesis these stages are operated in pool boiling mode (so that only the Cooper correlation is used). When a tube bank description is required on the water side, the geometry is:

- tube outer diameter: D_o ,
- cold-side flow area: $A_{\text{cold,flow}}$,
- number of rows: N_{rows} ,
- transverse and longitudinal pitches: S_T, S_L ,
- bundle arrangement: inline or staggered.

The water velocity, Reynolds and Prandtl numbers are:

$$V_w = \frac{\dot{m}_w}{\rho_w A_{\text{cold,flow}}}, \quad (5.69)$$

$$\text{Re}_w = \frac{\rho_w V_w D_o}{\mu_w}, \quad \text{Pr}_w = \frac{c_{p,w} \mu_w}{k_w}. \quad (5.70)$$

A Zukauskas-type banded correlation is then applied:

$$\text{Nu}_w = C \text{Re}_w^m \text{Pr}_w^n, \quad (5.71)$$

[6] where:

- C, m are selected from standard Zukauskas bands based on Re_w and the arrangement (inline or staggered),
- the exponent n is

$$n = \begin{cases} 0.36, & \text{Pr}_w \leq 10 \\ 0.25, & \text{Pr}_w > 10 \end{cases} \quad (5.72)$$

The raw Nusselt number is further modified by:

- a row factor $f_{\text{row}}(N_{\text{rows}})$ that accounts for the finite number of tube rows, and
- a spacing factor $\phi(S_T, S_L, D_o)$ that accounts for maximum velocity effects in the tube bank (greater constriction \Rightarrow higher HTC).

If Re_w falls outside the Zukauskas validity range, the model falls back to the Churchill Bernstein correlation for cross flow over a single cylinder:

$$\text{Nu}_w = 0.3 + \frac{0.62 \text{Re}_w^{1/2} \text{Pr}_w^{1/3}}{\left[1 + (0.4/\text{Pr}_w)^{2/3}\right]^{1/4}} \left[1 + \left(\frac{\text{Re}_w}{282000}\right)^{5/8}\right]^{4/5}. \quad (5.73)$$

[6]

The corresponding water side HTC for a tube-bank configuration is:

$$h_{w,\text{conv}}^{(\text{bank})} = \frac{\text{Nu}_w k_w}{D_o}. \quad (5.74)$$

[6]

When such a tube bank model is used inside the Chen formulation, h_{l_0} is taken from this $h_{w,\text{conv}}^{(\text{bank})}$.

5.7.4 Single tube and reversal chamber stages

Stages of kind `single_tube` and `reversal_chamber` correspond, on the water side, to external flow around one or more tubes within the drum/shell region. In the current thesis these are also operated in pool boiling mode (`pool_boiling = true`), so the Cooper pool boiling correlation described in the general formulation dominates their behavior. Nevertheless, the implementation includes external forced convection correlations for completeness.

For these stages the characteristic length for the water side is the tube outer diameter D_o , and the cold side flow area $A_{\text{cold,flow}}$ is defined by the drum cross section minus the tube area(s). When a cross flow description is used for single-phase or liquid only HTC:

- water velocity, Reynolds and Prandtl numbers:

$$V_w = \frac{\dot{m}_w}{\rho_w A_{\text{cold,flow}}}, \quad (5.75)$$

$$\text{Re}_w = \frac{\rho_w V_w D_o}{\mu_w}, \quad \text{Pr}_w = \frac{c_{p,w} \mu_w}{k_w}. \quad (5.76)$$

For a single tube in cross flow (or, by approximation, a relatively open bundle) a Churchill Bernstein style correlation is used:

$$\text{Nu}_w = 0.3 + \frac{0.62 \text{Re}_w^{1/2} \text{Pr}_w^{1/3}}{\left[1 + (0.4/\text{Pr}_w)^{2/3}\right]^{1/4}} \left[1 + \left(\frac{\text{Re}_w}{282000}\right)^{5/8}\right]^{4/5}, \quad (5.77)$$

[6] leading to

$$h_{w,\text{conv}}^{(\text{single})} = \frac{\text{Nu}_w k_w}{D_o}. \quad (5.78)$$

In reversal chamber segments, the tubes are bent, and the model applies the same base correlation multiplied by a curvature (bend) factor:

$$h_{w,\text{conv}}^{(\text{rev})} = \phi_{\text{bend}}(D_o, R_c) \frac{\text{Nu}_w k_w}{D_o}, \quad (5.79)$$

where R_c is the bend radius and $\phi_{\text{bend}} \geq 1$ is a modest enhancement (up to roughly 1.25) for tight bends, reflecting locally increased turbulence around the bend region.

In pool boiling operation these external convection correlations are only used implicitly inside the liquid only component h_{lo} when the Chen type formulation is invoked. For the main boiling sections in this thesis, however, the water side is predominantly controlled by the Cooper pool boiling correlation with $T_w = T_{\text{sat}}(p)$.

Chapter 6

Hydraulic Model

Hydraulic behavior is extracted directly from the solver through the per step pressure drop decomposition implemented in `heat/solver.py` (`_gas_dp_components`, `pressure_drop_gas`) and accumulated at the stage level in `heat/solver.py::solve_stage`.

The model divides gas side pressure losses into:

- Frictional losses
- Minor losses (inlet, outlet, bends, etc.)
- Total pressure drop (sum of the above)

6.1 Frictional losses

Gas and water sides

The per step frictional pressure drop follows a standard 1D Darcy formulation:

$$\Delta P_{\text{fric}} = -f \frac{\Delta x}{D_h} \left(\frac{\rho V^2}{2} \right) \quad (6.1)$$

[10]

Here:

- f is the Darcy friction factor,
- D_h is the relevant side hydraulic diameter ($D_h = \text{hot_Dh}$ for gas, $D_h = \text{cold_Dh}$ for water),
- ρ and V are local density and velocity on the relevant side,
- Δx is the current marching step length.

The friction factor is computed from Reynolds number and relative roughness via `_friction_factor`:

- Laminar ($\text{Re} < 2300$):

$$f = \frac{64}{\text{Re}} \quad (6.2)$$

[10]

- Transitional ($2300 \leq \text{Re} < 4000$): linear blend between laminar and turbulent values:

$$f = (1 - w)f_{\text{lam}} + wf_{\text{turb}}, \quad w = \frac{\text{Re} - 2300}{4000 - 2300} \quad (6.3)$$

[11]

- Turbulent ($\text{Re} \geq 4000$): Colebrook–White is solved iteratively, seeded by the Swamee–Jain explicit approximation.

Swamee–Jain seed (used as the initial guess):

$$f_{\text{SJ}} = \frac{0.25}{\left[\log_{10} \left(\frac{\varepsilon/D_h}{3.7} + \frac{5.74}{\text{Re}^{0.9}} \right) \right]^2} \quad (6.4)$$

[12]

Colebrook–White equation solved iteratively in the code:

$$\frac{1}{\sqrt{f}} = -2 \log_{10} \left(\frac{\varepsilon/D_h}{3.7} + \frac{2.51}{\text{Re}\sqrt{f}} \right) \quad (6.5)$$

[10]

The iteration is performed on $1/\sqrt{f}$ until convergence.

Local velocity and Reynolds number are evaluated using the side flow area A and properties:

$$V = \frac{\dot{m}}{\rho A}, \quad \text{Re} = \frac{\rho V D_h}{\mu} \quad (6.6)$$

Frictional losses are only applied for the economiser water side branch in `_water_dp_components`; for other stage kinds the current model sets $\Delta P_{\text{fric}} = 0$.

6.2 Minor losses

Minor losses are applied using per-stage catalogue K values and the standard dynamic-pressure formulation:

$$\Delta P_{\text{minor}} = -K_{\text{minor}} \left(\frac{\rho V^2}{2} \right) \quad (6.7)$$

[11]

The total minor-loss coefficient K_{minor} is assembled differently for gas and water sides, but applied through the same formulation.

Coefficient assembly

Gas side.

For each stage, the total loss coefficient is assembled from geometry and user inputs:

$$K_{\text{minor}} = K_{\text{contraction}} + K_{\text{expansion}} + K_{\text{bend}} \quad (6.8)$$

Where:

- $K_{\text{contraction}}$: accounts for sudden expansion of flow area (e.g. $\text{HX}_2 \rightarrow \text{HX}_3$), default = 0.5.
- $K_{\text{expansion}}$ (Borda–Carnot): losses caused by sudden expansion of flow area (e.g. $\text{HX}_1 \rightarrow \text{HX}_2$), default = 1.
- K_{bend} : losses due to gas flow rotation in reversal chambers, default = 0.

Water side.

Water-side minor losses are applied via per-stage catalogue coefficients in `heat/solver.py::_water_dp_cc`

- $K_{\text{cold,bend}} = \text{K_cold_bend}$
- $K_{\text{cold,inlet}} = \text{K_cold_inlet}$
- $K_{\text{cold,outlet}} = \text{K_cold_outlet}$

The bend loss is distributed uniformly across the n marching steps:

$$K_{\text{bend,per-step}} = \frac{K_{\text{cold,bend}}}{n} \quad (6.9)$$

The per-step assembled coefficient is:

$$K_{\text{minor}} = K_{\text{bend,per-step}} + \mathbb{1}_{i=0} K_{\text{cold,inlet}} + \mathbb{1}_{i=n-1} K_{\text{cold,outlet}} \quad (6.10)$$

Application

For both gas and water sides, the minor-loss pressure drop is computed using the local dynamic pressure:

$$V = \frac{\dot{m}}{\rho A}, \quad q = \frac{\rho V^2}{2}, \quad \Delta P_{\text{minor}} = -K_{\text{minor}} q \quad (6.11)$$

where A is the relevant side flow area ($A = \text{cold_flow_A}$ for water, gas-side area otherwise).

6.3 Total pressure drop

For each step, the total side pressure change is the sum of frictional and minor components:

$$\Delta P_{\text{total}} = \Delta P_{\text{fric}} + \Delta P_{\text{minor}} \quad (6.12)$$

[10]

This is what `pressure_drop_gas/water` return and what is applied to the streams in `update_gas/water_after_step`.

6.4 Coupling of ΔP into the energy solver

Gas/water pressure is updated step-wise using the same ΔP model:

$$P_{i+1} = P_i + \Delta P_{\text{total}}(P_i, T_i, \dots) \quad (6.13)$$

After each step:

1. The local gas/water state (T_i, P_i , composition) is used to evaluate ρ, μ, k , and c_p .
2. The friction factor and dynamic pressure are computed from these properties.
3. ΔP_{fric} and ΔP_{minor} are formed.
4. The updated pressure P_{i+1} is used for the next step.

In this way, compressibility enters through the pressure dependence of $\rho(T, P)$ and $\mu(T, P)$ and their effect on V, Re , and f .

Chapter 7

Performance

This section summarizes the boiler level performance obtained from the coupled combustion heat transfer simulation. All numerical values are extracted from the stages summary and boiler summary data produced by the post-processing step `heat/postproc.py`.

7.1 solution procedure

For any given operating conditions, the main solver `run_boiler_case()` performs an outer fixed point iteration, on boiler efficiency, and water mass flow:

1. The combustion sub-model called by `Combustor.run()`, returns:
 - the lower heating value based firing rate P_{LHV} ,
 - the total combustion heat release Q_{in} ,
 - the adiabatic flame temperature T_{ad} ,
 - the fully burnt flue-gas stream at burner exit.
2. Given a current efficiency guess $\eta^{(n)}$ and the combustion result, the corresponding feedwater/steam mass flow $\dot{m}_w^{(n)}$ is computed by `_water_mass_from_efficiency()` as

$$h_{\text{in}} = h_{\text{fw}}(P_{\text{fw}}), \quad h_{\text{steam}} = h_g(P_{\text{fw}}), \quad (7.1)$$

$$\Delta h = h_{\text{steam}} - h_{\text{in}}, \quad (7.2)$$

$$Q_{\text{target}}^{(n)} = \eta^{(n)} Q_{\text{in}}, \quad (7.3)$$

$$\dot{m}_w^{(n)} = \frac{Q_{\text{target}}^{(n)}}{\Delta h}. \quad (7.4)$$

3. A WaterStream with mass flow $\dot{m}_w^{(n)}$ is created and passed, together with the combustion flue gas GasStream and the drum/stage definitions, to the multi stage heat exchanger solver `run_hx()`.
4. `run_hx()` returns per stage and boiler level summary tables.
5. The new efficiency estimate is set to the indirect efficiency,

$$\eta^{(n+1)} := \eta_{\text{indirect}}^{(n)}, \quad (7.5)$$

And the procedure is repeated until the change in water mass flow between iterations is below the specified tolerance

$$|\dot{m}_w^{(n)} - \dot{m}_w^{(n-1)}| < 10^{-3} \text{ kg/s}, \quad (7.6)$$

or a maximum number of iterations is reached.

At convergence, returning:

- converged water/steam mass flow $\dot{m}_{w,\text{base}}$,
- converged indirect efficiency $\eta_{\text{indirect},\text{base}}$,

together with the corresponding boiler summary quantities (stack temperature, total pressure drop, etc.). These and more are exported to CSV as `boiler_summary.csv` and `stages_summary.csv`.

7.2 Energy balance

The total useful heat transferred from the flue gas to the water/steam side is obtained by integrating the local line heat flux $q'(x)$ over all stages:

$$Q_{\text{useful}} = \sum_{k=1}^6 Q_{\text{stage},k} = \sum_{k=1}^6 \int_q' (x) dx \quad (7.7)$$

The total input heat from combustion Q_{in} is taken from the combustion module as the rate of heat release from complete fuel burnout:

7.3 Efficiency

Two boiler efficiencies are reported:

- Direct efficiency (LHV):

$$\eta_{\text{direct}} = \frac{Q_{\text{useful}}}{P_{\text{LHV}}} \quad (7.8)$$

- Indirect efficiency:

$$\eta_{\text{indirect}} = 1 - \frac{Q_{\text{losses}}}{Q_{\text{in}}} \quad (7.9)$$

7.4 Water/Steam flow rate convergence

The water/steam mass flow rate is obtained iteratively from an assumed overall boiler efficiency and the combustion heat input. At each iteration n the code:

1. Assumes an efficiency $\eta^{(n)}$.
2. Computes the target useful duty:

$$Q_{\text{target}}^{(n)} = \eta^{(n)} Q_{\text{in}} \quad (7.10)$$

3. Determines the required water mass flow $\dot{m}_w^{(n)}$ from the enthalpy rise between feed-water and saturated steam at drum pressure:

$$\dot{m}_w^{(n)} = \frac{Q_{\text{target}}^{(n)}}{h_{\text{steam}}(P_{\text{drum}}) - h_{\text{fw}}} \quad (7.11)$$

4. Runs the full multi-stage heat-exchanger model with $\dot{m}_w^{(n)}$ and reads back the resulting indirect efficiency $\eta_{\text{indirect}}^{(n)}$.
5. Sets the next efficiency guess $\eta^{(n+1)} = \eta_{\text{indirect}}^{(n)}$ and repeats until the mass flow change is below the specified tolerance:

$$|\dot{m}_w^{(n)} - \dot{m}_w^{(n-1)}| < 10^{-3} \text{ kg/s} \quad (7.12)$$

7.5 Stage level performance

Stage level performance table returned by the post processor `heat/postproc.py`. For each stage k the following quantities are available:

- Heat duty: `Q_stage[MW]`
- Overall conductance: `UA_stage[MW/K]`
- Gas inlet/outlet temperatures: `gas_in_T[°C]`, `gas_out_T[°C]`
- Water inlet/outlet temperatures: `water_in_T[°C]`, `water_out_T[°C]`
- Gas side pressure drops: `ΔP_stage_fric[Pa]`, `ΔP_stage_minor[Pa]`, `ΔP_stage_total[Pa]`

- Decomposition of duty into convection and radiation: $Q_{\text{conv_stage}}[\text{MW}]$, $Q_{\text{rad_stage}}[\text{MW}]$

Table 7.1: Stages summary results.

Kind	$T_{g,\text{in}}$ [°C]	$T_{g,\text{out}}$ [°C]	$T_{w,\text{in}}$ [°C]	$T_{w,\text{out}}$ [°C]	Q_{stage} [MW]	UA_{stage} [MW/K]	ΔP_{stage} [Pa]
single tube	[·]	[·]	[·]	[·]	[·]	[·]	[·]
reversal ch.	[·]	[·]	[·]	[·]	[·]	[·]	[·]
tube bank	[·]	[·]	[·]	[·]	[·]	[·]	[·]
reversal ch.	[·]	[·]	[·]	[·]	[·]	[·]	[·]
tube bank	[·]	[·]	[·]	[·]	[·]	[·]	[·]
economizer	[·]	[·]	[·]	[·]	[·]	[·]	[·]

7.6 Boiler performance

The overall boiler performance is summarized using the boiler summary table, supplied by `heat/postproc.py`:

Table 7.2: Boiler summary results.

Quantity	Symbol	Value
Fuel firing (LHV basis)	P_{LHV}	
Total heat input (combustion)	Q_{in}	
Useful heat to water/steam	Q_{useful}	
Direct efficiency (LHV basis)	η_{direct}	
Indirect efficiency	η_{indirect}	
Stack gas temperature	T_{stack}	
Gas side friction loss	ΔP_{fric}	
Gas side minor losses	ΔP_{minor}	
Total gas side pressure drop	ΔP_{tot}	
Total convective heat transfer	Q_{conv}	
Total radiative heat transfer	Q_{rad}	

These boiler level results provide the basis for the sensitivity analysis in Section 8 and for comparing alternative design or operating scenarios.

Chapter 8

Boiler performance analysis

The present chapter evaluates the thermal and hydraulic performance of the fire tube boiler model based on steady state simulations of a reference control case and systematic parameter variations. The analysis is structured to introduce the control case first and then to discuss the influence of excess air factor, fuel mass flow, and drum pressure, followed by a stage wise interpretation of heat transfer and gas side hydraulics.

8.1 Control case

Table 8.1: Control case performance.

Control	control
fuel mass flow[kg/s]	0.1
air flow[kg/s]	1.77
excess air ratio[-]	1.1
water flow[kg/s]	1.78
steam capacity[t/h]	7.45
$\eta_{\text{direct}}[-]$	0.89
$\eta_{\text{indirect}}[-]$	0.89
Conductance [MW/K]	0.01
Useful heat [MW]	4.17
pressure drop total[Pa]	-74.96
LHV [MJ/kg]	46.97
Firing rate [MW]	4.7
Adiabatic temperature [°C]	1900.61
stack temperature[°C]	181.41

The control case corresponds to the nominal design operation introduced in the previous chapters and serves as the reference state for all relative comparisons in this chapter.

8.2 Global boiler performance

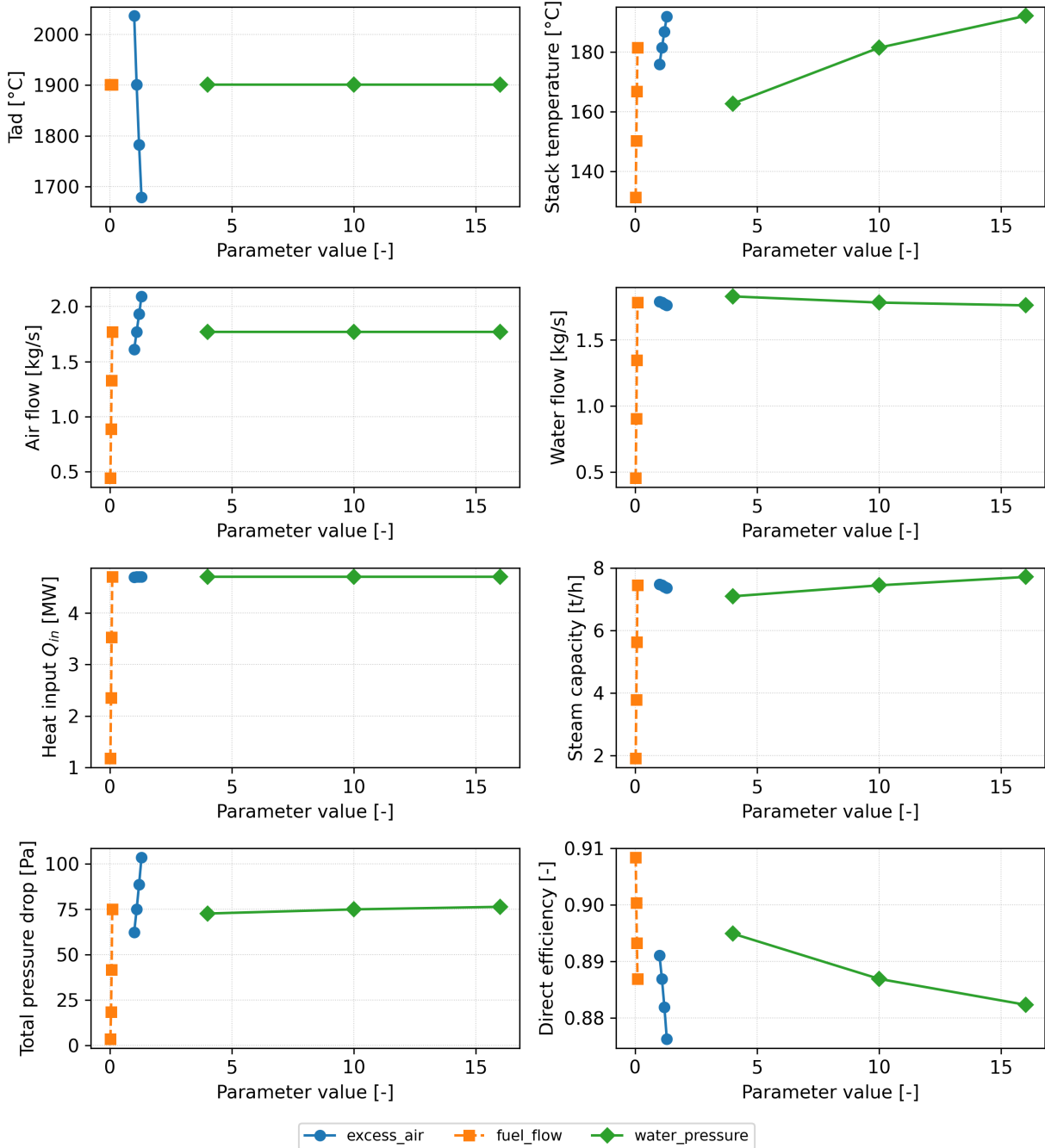


Figure 8.1: Overview of key boiler performance indicators for all parameter groups

This figure provides a compact summary of how the different parameter groups shift the global performance relative to the control case introduced above. In the remainder of the chapter, each parameter group is analyzed separately.

8.3 Influence of excess air factor

$$\lambda = [1.0, 1.1, 1.2, 1.3] [-] \quad (8.1)$$

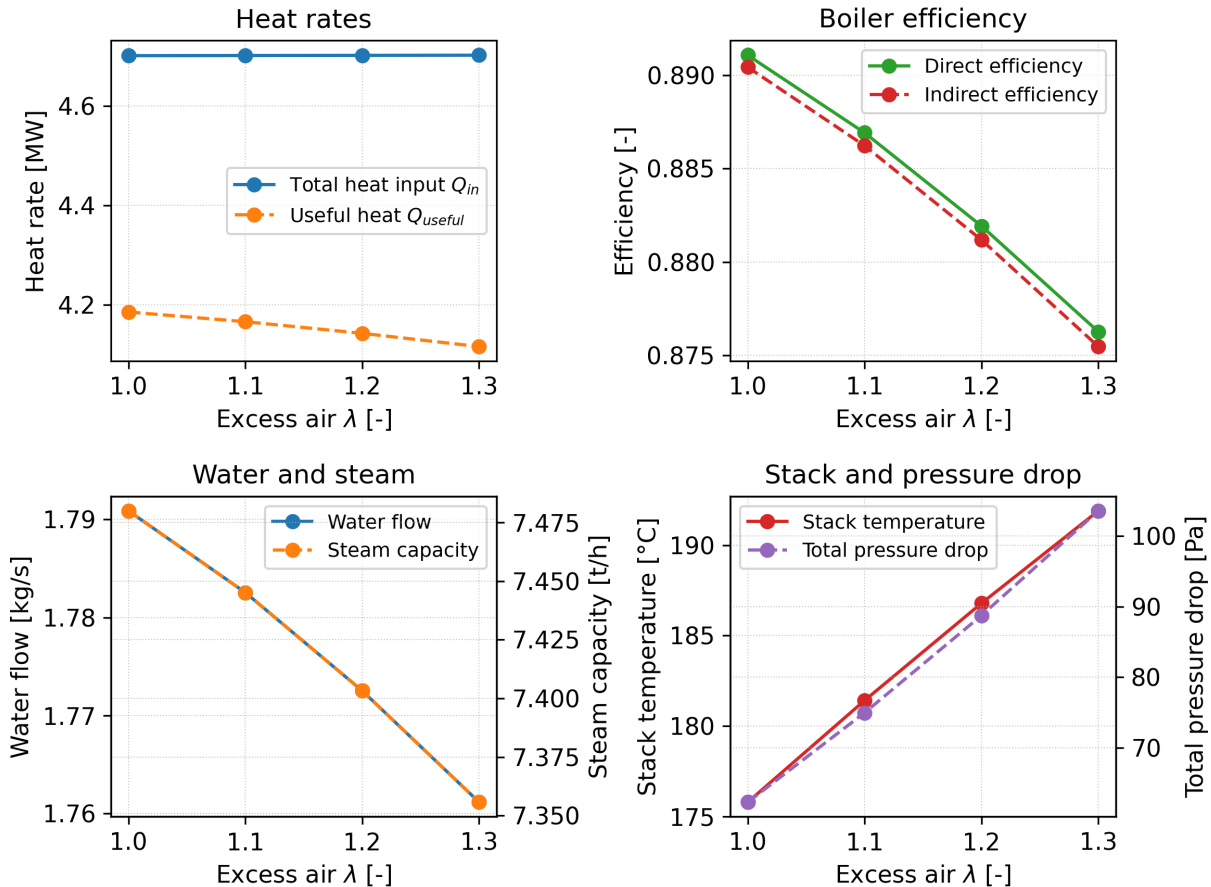


Figure 8.2: Boiler performance as a function of excess air factor

Decreasing λ towards stoichiometric conditions increases T_{ad} and the fraction of duty absorbed in the radiant section, while increasing λ leads to higher stack losses due to additional sensible heat in the flue gas.

Table 8.2: Excess air performance analysis.

Excess air [-]	1.00	1.10	1.20	1.30
fuel mass flow[kg/s]	0.1	0.1	0.1	0.1
air flow[kg/s]	1.61	1.77	1.93	2.09
excess air ratio[-]	1	1.1	1.2	1.3
water flow[kg/s]	1.79	1.78	1.77	1.76
steam capacity[t/h]	7.48	7.45	7.4	7.36

Excess air [-]	1.00	1.10	1.20	1.30
$\eta_{\text{direct}}[-]$	0.89	0.89	0.88	0.88
$\eta_{\text{indirect}}[-]$	0.89	0.89	0.88	0.88
Conductance [MW/K]	0.01	0.01	0.01	0.01
Input heat [MW]	4.7	4.7	4.7	4.7
Useful heat [MW]	4.19	4.17	4.14	4.12
pressure drop fric total[Pa]	-49.46	-59.43	-70.27	-81.95
pressure drop minor total[Pa]	-12.82	-15.54	-18.49	-21.65
pressure drop total[Pa]	-62.28	-74.96	-88.76	-103.6
LHV [MJ/kg]	46.97	46.97	46.97	46.97
Firing rate [MW]	4.7	4.7	4.7	4.7
Adiabatic temperature [°C]	2036.41	1900.61	1782.51	1678.83
stack temperature[°C]	175.78	181.41	186.78	191.89

Key observations from tbl. 8.2 are:

- Increasing excess air from $\lambda = 1.0$ to $\lambda = 1.3$ decreases the direct efficiency from about 0.891 to 0.876 ($\approx 1.5\%$).
- Over the same range, stack temperature increases from approximately 176 °C to 192 °C, indicating higher sensible heat losses with the flue gas.
- The total gas side pressure drop rises from about -62 Pa to -104 Pa as air flow and hence gas mass flow increase.
- The useful heat Q_{useful} decreases slightly with λ , while the overall conductance UA increases modestly due to higher gas side Reynolds numbers.

8.4 Influence of fuel mass flow

$$\dot{m}_{\text{fuel}} = [0.10, 0.075, 0.050, 0.025] \frac{\text{kg}}{\text{s}} \quad (8.2)$$

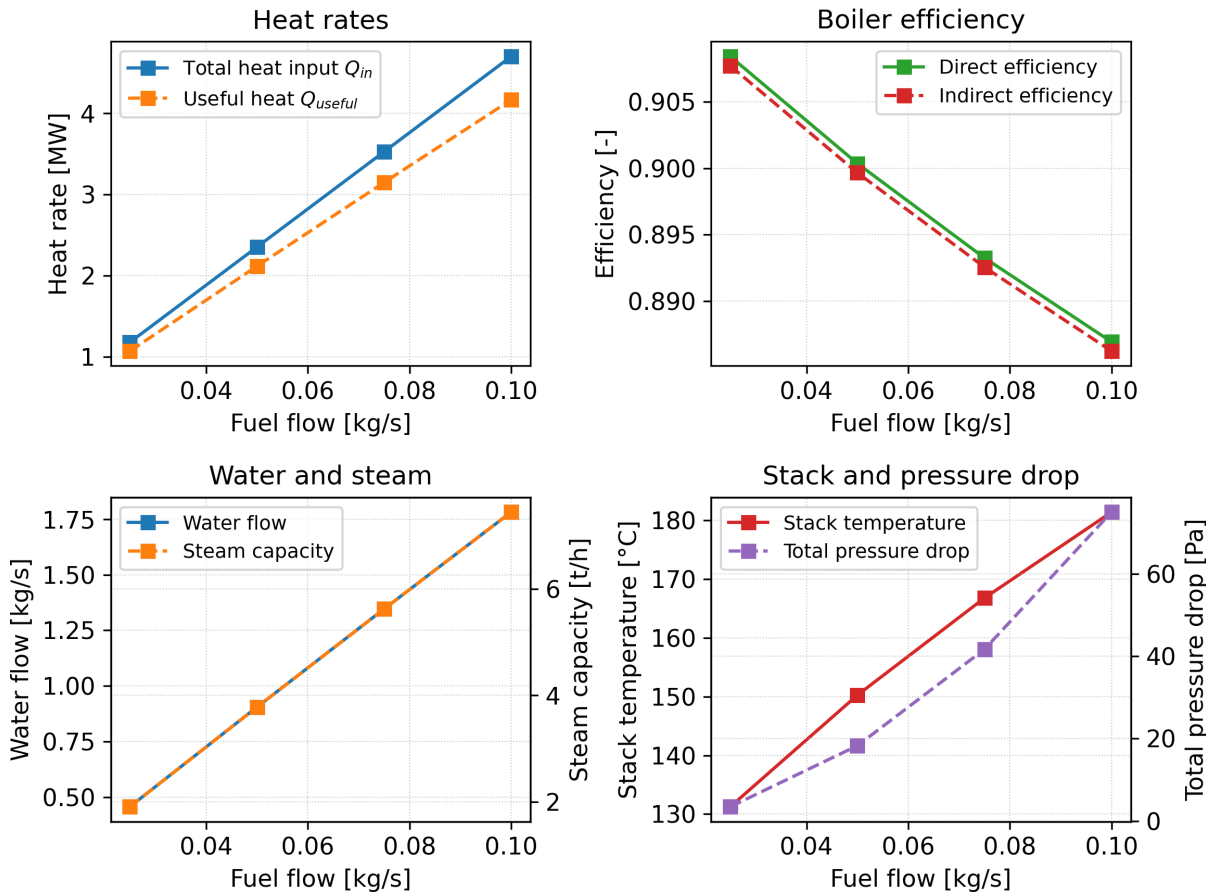


Figure 8.3: Boiler performance as a function of fuel mass flow

The fuel mass flow sweep explores operation between 25% and 100% of nominal firing rate. As the load increases, the higher gas mass flow and gas side Reynolds numbers enhance convective heat transfer, particularly in HX3 and HX5, while also increasing gas side pressure drops and velocities.

Table 8.3: Fuel flow performance analysis.

Fuel flow [kg/s]	0.02	0.05	0.08	0.10
fuel mass flow[kg/s]	0.02	0.05	0.08	0.1
air flow[kg/s]	0.44	0.89	1.33	1.77
excess air ratio[-]	1.1	1.1	1.1	1.1

Fuel flow [kg/s]	0.02	0.05	0.08	0.10
water flow[kg/s]	0.46	0.9	1.35	1.78
steam capacity[t/h]	1.91	3.78	5.62	7.45
$\eta_{\text{direct}}[-]$	0.91	0.9	0.89	0.89
$\eta_{\text{indirect}}[-]$	0.91	0.9	0.89	0.89
Conductance [MW/K]	0	0.01	0.01	0.01
Input heat [MW]	1.18	2.35	3.53	4.7
Useful heat [MW]	1.07	2.11	3.15	4.17
pressure drop fric total[Pa]	-2.79	-15.03	-33.54	-59.43
pressure drop minor total[Pa]	-0.68	-3.25	-8.13	-15.54
pressure drop total[Pa]	-3.47	-18.28	-41.67	-74.96
LHV [MJ/kg]	46.97	46.97	46.97	46.97
Firing rate [MW]	1.17	2.35	3.52	4.7
Adiabatic temperature [°C]	1900.61	1900.61	1900.61	1900.61
stack temperature[°C]	131.25	150.24	166.78	181.41

Key observations from tbl. 8.3 are:

- As fuel mass flow increases from 0.025 to 0.1 kg/s (25% to 100% load), steam capacity rises from about 1.9 t/h to 7.4 t/h.
- The direct efficiency decreases slightly with load, from around 0.908 at 25% load to 0.887 at 100% load.
- The gas-side pressure drop increases strongly with load, from about -3 Pa to -75 Pa, reflecting the approximate quadratic dependence on gas mass flow.
- Stack temperature increases from roughly 131 °C at 25% load to 181 °C at full load, which indicates less complete heat recovery at high firing rates.

8.5 Influence of drum pressure

$$P_{\text{Drum}} = [4.0, 10.0, 16.0] \text{ bar} \quad (8.3)$$

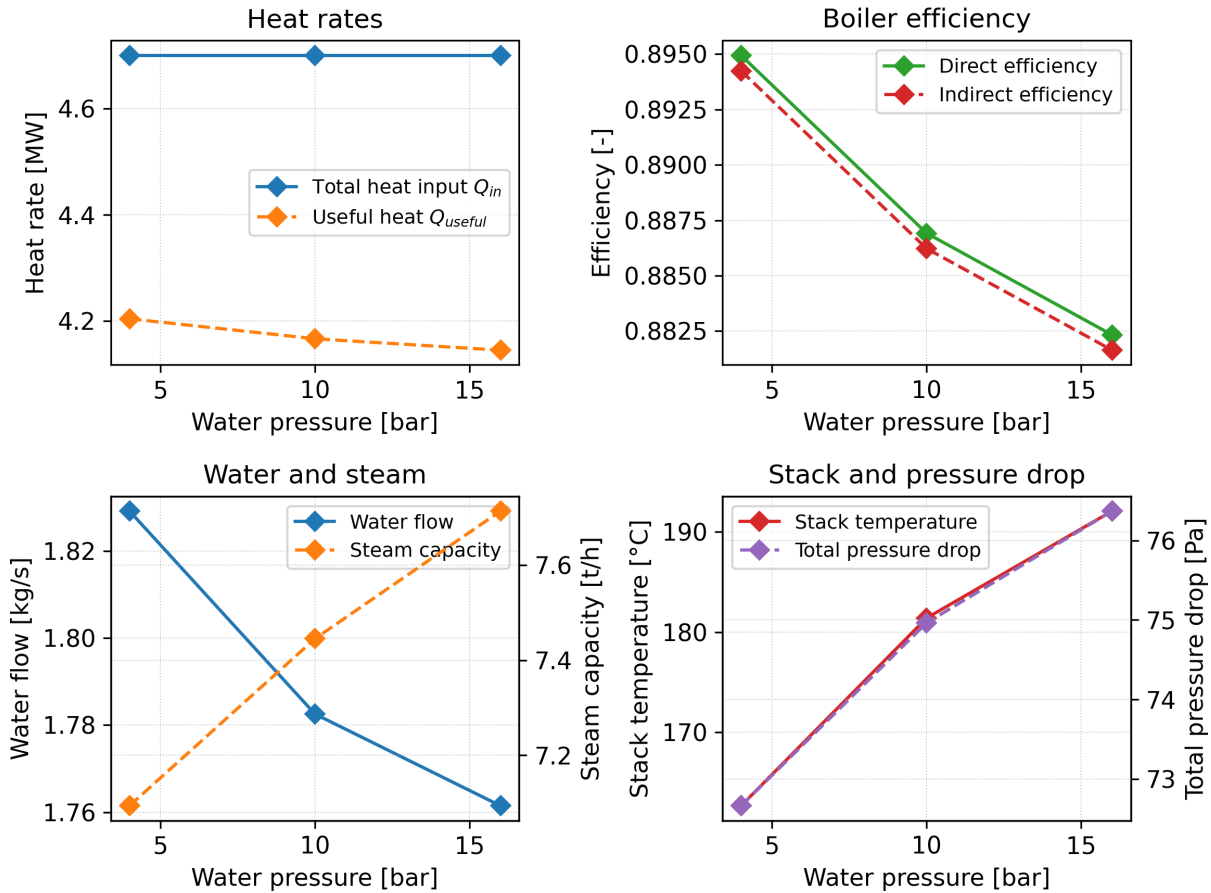


Figure 8.4: Boiler performance as a function of drum pressure

The drum pressure variation modifies the steam saturation temperature and thus the driving temperature difference between flue gas and water or steam on each heat exchanger surface.

Table 8.4: Drum pressure performance analysis.

Water pressure [bar]	4.00	10.00	16.00
fuel mass flow[kg/s]	0.1	0.1	0.1
air flow[kg/s]	1.77	1.77	1.77
excess air ratio[-]	1.1	1.1	1.1
water flow[kg/s]	1.83	1.78	1.76
steam capacity[t/h]	7.09	7.45	7.71

Water pressure [bar]	4.00	10.00	16.00
$\eta_{\text{direct}}[-]$	0.89	0.89	0.88
$\eta_{\text{indirect}}[-]$	0.89	0.89	0.88
Conductance [MW/K]	0.01	0.01	0.01
Input heat [MW]	4.7	4.7	4.7
Useful heat [MW]	4.2	4.17	4.14
pressure drop fric total[Pa]	-57.2	-59.43	-60.78
pressure drop minor total[Pa]	-15.46	-15.54	-15.59
pressure drop total[Pa]	-72.66	-74.96	-76.37
LHV [MJ/kg]	46.97	46.97	46.97
Firing rate [MW]	4.7	4.7	4.7
Adiabatic temperature [°C]	1900.61	1900.61	1900.61
stack temperature[°C]	162.68	181.41	192.08

Key observations from tbl. 8.4 are:

- At fixed fuel and air flows, increasing drum pressure from 4 bar to 16 bar increases steam capacity from about 7.1 t/h to 7.7 t/h due to higher steam enthalpy.
- The direct efficiency decreases from about 0.895 at 4 bar to 0.882 at 16 bar, as higher water/steam temperatures reduce the driving temperature difference on the gas side.
- Stack temperature increases from approximately 163 °C at 4 bar to 192 °C at 16 bar, reflecting the reduced potential for additional heat recovery.
- Gas-side pressure drops remain essentially unchanged with drum pressure because gas mass flow and gas-side geometry are not affected.

8.6 Stage wise heat transfer behavior

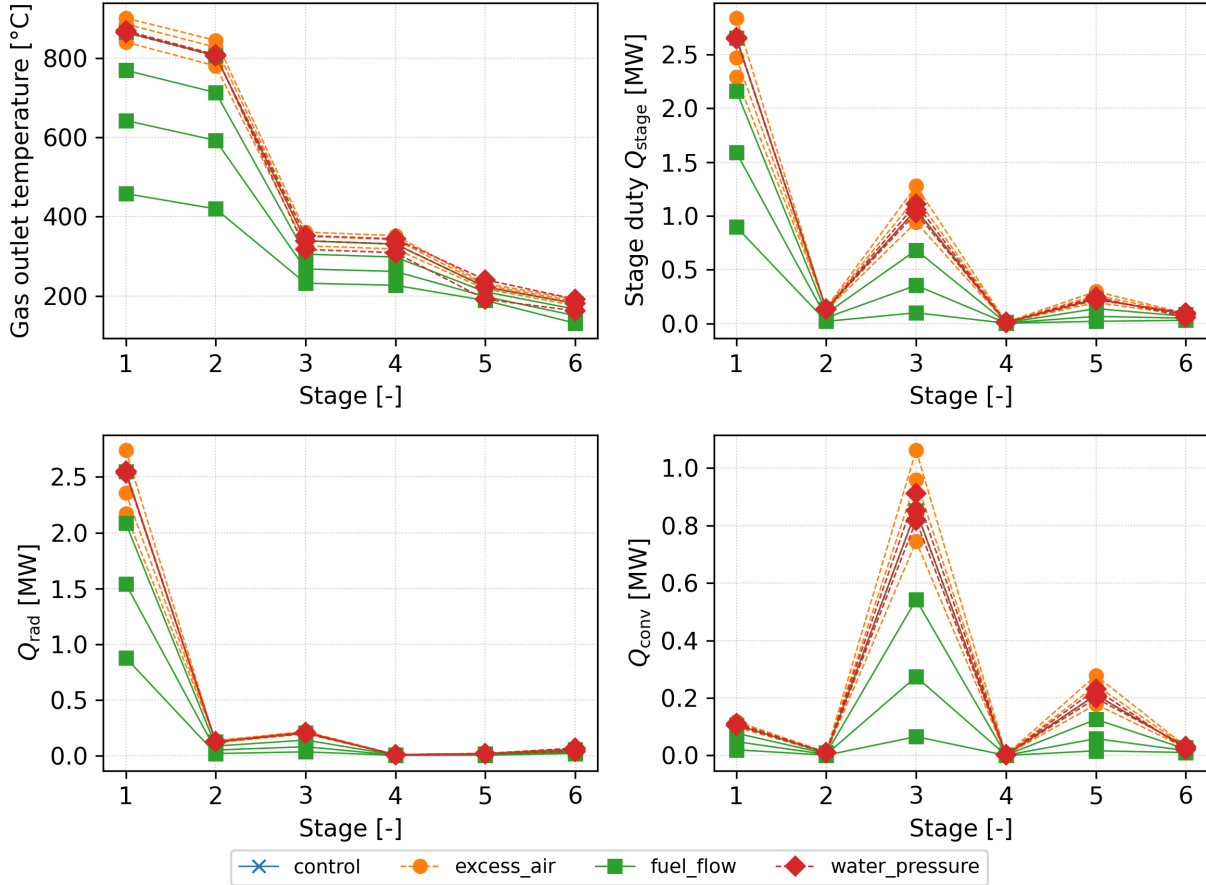


Figure 8.5: Stage wise heat transfer profile

Variations in λ primarily affect Q_{stage} and UA in the radiant section and the first convective bank, while load changes affect both the magnitude and the distribution of duty along the gas path. The drum pressure variation, alters the effective UA utilization in each stage.

Variations in λ primarily affect Q_{stage} and UA in the radiant section (HX1) and the first convective bank (HX3). At lower excess air (higher T_{ad}), these stages absorb a larger fraction of the total duty, while the downstream convective banks see a reduced relative share. Increasing λ shifts some duty towards the later convective stages but also raises stack losses.

Load changes affect both the magnitude and the distribution of duty along the gas path. At low load, duty is concentrated in the early stages and the later convective banks are underutilized, resulting in low gas velocities and small pressure drops. As load increases, Q_{stage} grows in all stages, with a particularly strong relative increase in the convective banks where the higher gas-side Reynolds numbers strongly enhance UA .

The drum pressure variation mainly alters the effective utilization of UA in each stage rather than the absolute UA values. Higher drum pressure increases water/steam temperature and therefore reduces the local temperature differences, especially in the later convective stages where gas temperatures are already low. This leads to a shift of the effective heat transfer towards the upstream stages and contributes to the observed increase in stack temperature at high pressure.

8.7 Gas side hydraulics and heat transfer decomposition

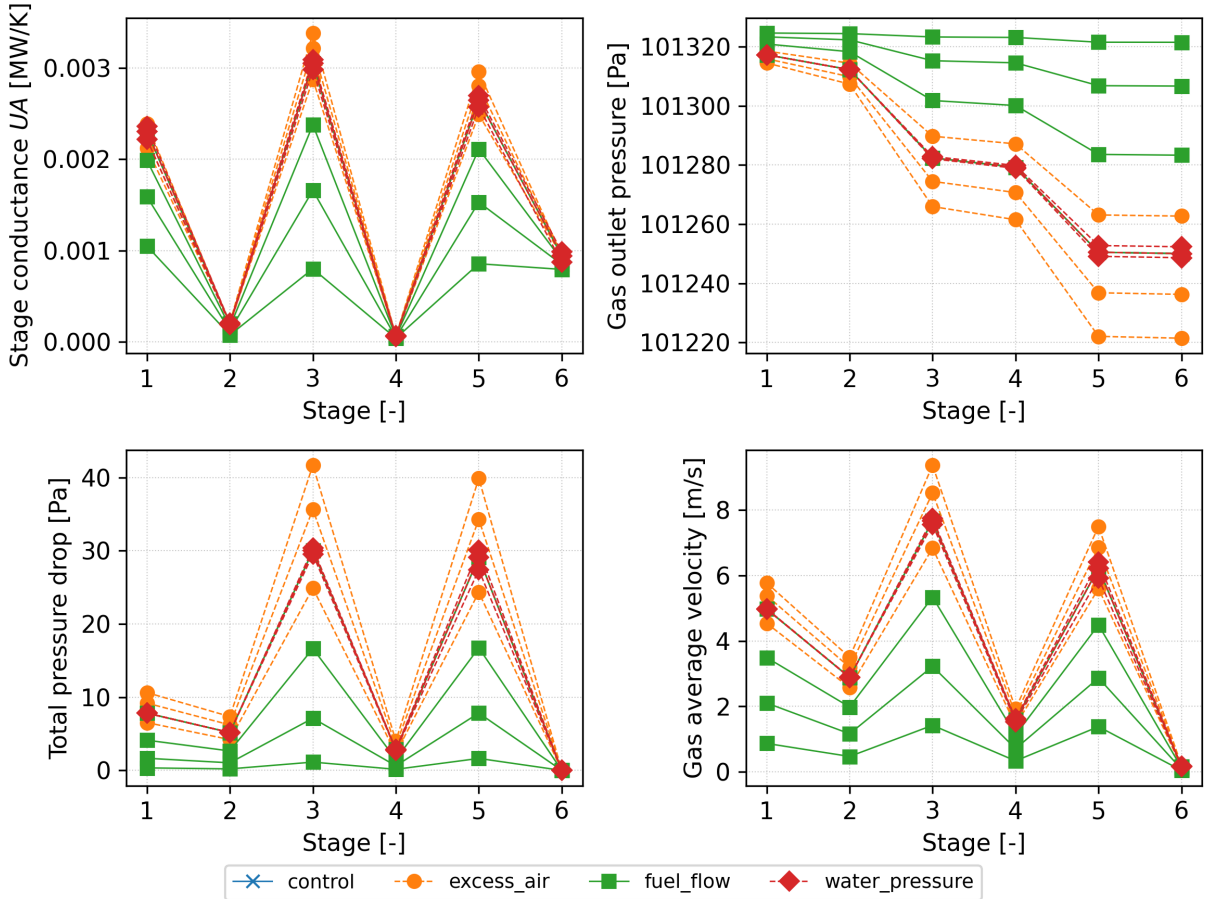


Figure 8.6: Stage wise hydraulics and conductance profile

The figure clarifies how changes in fuel mass flow and excess air factor translate into different velocity and pressure profiles and how this in turn influences heat transfer modes in each heat exchanger. The presented data enable a consistent interpretation of how hydraulic margins evolve with operating point and how close individual stages approach practical constraints such as allowable gas velocity or pressure drop. In combination with the previous plots, this information supports the identification of an operating window that balances efficiency, steam conditions, and hydraulic safety.

Figure clarifies how changes in fuel mass flow and excess air factor translate into different velocity and pressure profiles and how this in turn influences heat transfer modes in each heat exchanger. For increasing load, the gas velocity in all stages increases approximately in proportion to mass flow, and the stage-wise pressure drops increase roughly with the square of velocity. This behavior is most pronounced in the convective tube banks, where friction losses dominate.

At high load and high excess air, the maximum stage-wise gas velocity approaches the upper range of typical design values for fire tube boilers, while the total pressure drop remains within the available fan head. At low load, gas velocities are small, especially in the last convective stage, which may limit convective heat transfer and affect combustion stability in practice.

The presented data therefore enable a consistent interpretation of how hydraulic margins evolve with operating point and how close individual stages approach practical constraints such as allowable gas velocity or pressure drop. In combination with the previous plots, this information supports the identification of an operating window that balances efficiency, steam conditions, and hydraulic safety.

Chapter 9

Conclusion

This thesis developed and validated a coupled combustion–heat-transfer–hydraulics model for a three-pass fire-tube industrial shell boiler. The framework integrates detailed fuel–air combustion using Cantera, multi-stage radiative and convective heat-transfer modelling across six sequential heat-exchange sections, and a resistance-based hydraulic model for gas-side pressure losses. The approach captures the dominant physical mechanisms governing boiler performance while remaining computationally tractable for iterative operating-point calculations and sensitivity studies.

The modelling framework successfully reproduces the expected qualitative behaviour of industrial shell boilers:

- The adiabatic flame temperature T_{ad} is predicted from full HP-equilibrium chemistry, providing a physically consistent upper-bound reference state for the flue gas.
- Radiative transfer in the furnace (HX_1) dominates high-temperature heat exchange, while the downstream tube banks (HX_3 and HX_5) provide the bulk of convective duty.
- The economiser (HX_6) is correctly characterised as a single-phase internal flow exchanger, with performance governed largely by gas-side convection.

At the boiler scale, the simulation produces converged operating conditions by solving a fixed-point iteration linking efficiency, combustion heat input, and steam mass flow. This procedure captures the inherent coupling between water/steam generation and flue-gas cooling, ensuring global energy consistency.

The sensitivity studies demonstrate three principal findings:

1. **Excess air ratio λ .**

Efficiency exhibits a shallow optimum close to the design value. Increasing λ beyond this point lowers furnace temperatures, reduces radiative heat transfer, increases stack losses, and raises overall gas-side pressure drop. The model quantifies these effects and highlights the operational importance of controlling excess air.

2. **Drum/feedwater pressure.**

Pressure mainly influences *steam quantity* rather than *efficiency*. Higher pressures

increase saturation temperature and reduce latent heat, leading to lower steam mass flow for the same heat input. The indirect efficiency varies only mildly across the investigated pressure range.

3. Firing rate (fuel mass flow).

Useful duty and steam flow scale nearly linearly with firing rate over a broad operating window. Efficiency remains relatively stable at mid-loads, with penalties at both low and high firing rates due to deteriorated heat-transfer coefficients and increased stack temperatures. Gas-side pressure drop increases strongly with load, reflecting the quadratic dependence on velocity.

Overall, the model provides a physics-based, modular, and extensible framework suitable for performance assessment, operational optimisation, and early-stage design exploration of industrial shell boilers. It enables quantitative evaluation of how geometry, combustion conditions, and operating parameters influence heat-transfer distribution, steam capacity, efficiency, and hydraulic behaviour.

Future work could extend the present model by incorporating:

- transient operation and burner cycling,
- advanced radiation models (spectral or WSGG-based),
- two-phase water/steam circulation modelling within the pressure parts,
- fouling, slagging, and degradation effects over time,
- NO_x formation and emissions modelling coupled to flame-temperature predictions.

Such extensions would further enhance the model's fidelity and applicability across a wider range of industrial boiler configurations and operating regimes.

Appendix A

config and input

A.1 Operating condition (config/operation.yaml)

Table: Operation Conditions | property | value | unit || excess air ratio | 1.1 | dimensionless |

A.2 Air input properties (config/air.yaml)

Table: Air Properties | property | value | unit || T | 300.0 | kelvin || P | 101325 | Pa || composition O₂ | 0.2095 | dimensionless || composition N₂ | 0.7808 | dimensionless || composition Ar | 0\$0.0093 | dimensionless || composition CO₂ | 0.0004 | dimensionless || composition H₂O | 0.0 | dimensionless |

A.3 Fuel properties and composition (config/fuel.yaml)

Table: Fuel Properties | property | value | unit || T | 300.0 | kelvin || P | 101325 | Pa || mass flow | 0.1 | kg/s || composition CH₄ | 0.80 | dimensionless || composition C₂H₆ | 0.10 | dimensionless || composition C₃H₈ | 0.04 | dimensionless || composition C₄H₁₀ | 0.01 | dimensionless || composition H₂S | 0.01 | dimensionless || composition N₂ | 0.02 | dimensionless || composition CO₂ | 0.01 | dimensionless || composition H₂O | 0.01 | dimensionless |

A.4 Water input properties (config/water.yaml)

Table: Water Properties | property | value | unit || enthalpy | 300000 | J/kg || pressure | 1000000 | Pa || composition H₂O | 1.0 | dimensionless |

A.5 Drum geometry and wall properties (config/drum.yaml)

Table: Drum Properties | property | value | unit | inner diameter | 4.5 | m | length | 5.0 | m | wall inner roughness | 5 | micrometer | foulng thickness | 0.0001 | m | foulng conductivity | 0.2 | W/m/K |

A.6 Heat exchanger stages (config/stages.yaml)

Table: HX 1 | property | value | unit | kind | single tube | pool boiling | true | inner diameter | 1.4 | m | inner length | 5.276 | m | wall thickness | 0.0029 | m | wall conductivity | 16 | W/m/K | wall inner roughness | 0.5 | micrometer | wall inner emissivity | 0.80 | dimensionless | wall inner foulng thickness | 0.0001 | m | wall inner foulng conductivity | 0.20 | W/m/K | wall outer roughness | 0.5 | micrometer | wall outer emissivity | 0.80 | dimensionless | wall outer foulng thickness | 0.0001 | m | wall outer foulng conductivity | 0.20 | W/m/K |

Table: HX 2 | property | value | unit | kind | reversal chamber | pool boiling | true | inner diameter | 1.6 | m | inner length | 0.8 | m | curvature radius | 0.8 | m | wall thickness | 0.0029 | m | wall conductivity | 16 | W/m/K | wall inner roughness | 0.5 | micrometer | wall inner emissivity | 0.80 | dimensionless | wall inner foulng thickness | 0.0001 | m | wall inner foulng conductivity | 0.20 | W/m/K | wall outer roughness | 0.5 | micrometer | wall outer emissivity | 0.80 | dimensionless | wall outer foulng thickness | 0.0001 | m | wall outer foulng conductivity | 0.20 | W/m/K |

Table: HX 3 | property | value | unit | kind | tube bank | pool boiling | true | inner diameter | 0.076 | m | inner length | 4.975 | m | tubes number | 118 | dimensionless | arrangement | staggered | rows number | 6 | dimensionless | ST | 0.11 | m | SL | 0.11 | m | baffle spacing | 0.075 | m | shell inner diameter | 1.80 | m | baffle cut | 0.25 | dimensionless | bundle clearance | 0.010 | m | wall thickness | 0.0029 | m | wall conductivity | 16 | W/m/K | wall inner roughness | 0.5 | micrometer | wall inner emissivity | 0.80 | dimensionless | wall inner foulng thickness | 0.0001 | m | wall inner foulng conductivity | 0.20 | W/m/K | wall outer roughness | 0.5 | micrometer | wall outer emissivity | 0.80 | dimensionless | wall outer foulng thickness | 0.0001 | m | wall outer foulng conductivity | 0.20 | W/m/K |

Table: HX 4 | property | value | unit | kind | reversal chamber | pool boiling | true | inner diameter | 1.6 | m | inner length | 0.8 | m | curvature radius | 0.8 | m | wall thickness | 0.0029 | m | wall conductivity | 16 | W/m/K | wall inner roughness | 0.5 | micrometer | wall inner emissivity | 0.80 | dimensionless | wall inner foulng thickness | 0.0001 | m | wall inner foulng conductivity | 0.20 | W/m/K | wall outer roughness | 0.5 | micrometer | wall outer emissivity | 0.80 | dimensionless | wall outer foulng thickness | 0.0001 | m | wall outer foulng conductivity | 0.20 | W/m/K |

Table: HX 5 | property | value | unit | kind | tube bank | pool boiling | true | inner diameter | 0.076 | m | inner length | 5.620 | m | tubes number | 100 | dimensionless | arrangement | staggered | rows number | 6 | dimensionless | ST | 0.11 | m | SL | 0.11 | m | baffle spacing | 0.075 | m | shell inner diameter | 1.80 | m | baffle cut | 0.25 | dimensionless | bundle clearance | 0.010 | m | wall thickness | 0.0029 | m | wall conductivity | 16 | W/m/K | wall inner roughness | 0.5 | micrometer | wall inner emissivity | 0.80 | dimensionless | wall inner foulng thickness | 0.0001 | m | wall inner foulng conductivity | 0.20 | W/m/K | wall outer roughness | 0.5 | micrometer | wall outer emissivity | 0.80 | dimensionless | wall outer foulng thickness | 0.0001 | m | wall outer foulng conductivity | 0.20 | W/m/K |

| 0.11 | m || baffle spacing | 0.075 | m || shell inner diameter | 1.80 | m || baffle cut
 | 0.25 | dimensionless || bundle clearance | 0.010 | m || wall thickness | 0.0029 | m ||
 | wall conductivity | 16 | W/m/K || wall inner roughness | 0.5 | micrometer || wall inner
 emissivity | 0.80 | dimensionless || wall inner fouling thickness | 0.0001 | m || wall inner
 fouling conductivity | 0.20 | W/m/K || wall outer roughness | 0.5 | micrometer || wall outer
 emissivity | 0.80 | dimensionless || wall outer fouling thickness | 0.0001 | m || wall outer
 fouling conductivity | 0.20 | W/m/K |

Table: HX 6 | property | value | unit | kind | economizer | || pool boiling | false | || inner
 diameter | 0.076 | m || inner length | 7.5 | m || tubes number | 160 | dimensionless ||
 layout | triangular | | arrangement | inline | | rows number | 4 | dimensionless || ST |
 0.123 | m || SL | 0.123 | m || baffle spacing | 0.085 | m || shell inner diameter | 1.80 |
 m || baffle cut | 0.25 | dimensionless || bundle clearance | 0.010 | m || wall thickness |
 0.0025 | m || wall conductivity | 30 | W/m/K || wall inner roughness | 0.5 | micrometer ||
 wall inner emissivity | 0.80 | dimensionless || wall inner fouling thickness | 0.0 | m || wall
 inner fouling conductivity | 0.20 | W/m/K || wall outer roughness | 0.5 | micrometer || wall
 outer emissivity | 0.80 | dimensionless || wall outer fouling thickness | 0.0 | m || wall outer
 fouling conductivity | 0.20 | W/m/K |

References

- [1] International Organization for Standardization, "ISO 6976: Natural gas – calculation of calorific values, density, relative density and wobbe index," ISO, Geneva, Switzerland, 2016.
- [2] B. J. McBride, S. Gordon, and M. A. Reno, "Coefficients for calculating thermodynamic and transport properties of individual species," NASA Glenn Research Center, Cleveland, Ohio, NASA/TP-2002-211556, 2002.
- [3] R. D. Johnson *et al.*, "NIST chemistry WebBook, NIST standard reference database number 69." <https://webbook.nist.gov/chemistry/>; National Institute of Standards; Technology, Gaithersburg, MD, 2024.
- [4] S. R. Turns, *An introduction to combustion: Concepts and applications*, 3rd ed. McGraw-Hill, 2012.
- [5] B. J. McBride, S. Gordon, and M. A. Reno, *Coefficients for calculating thermodynamic and transport properties of individual species*. in NASA reference publication 1311. NASA Glenn Research Center, 1993.
- [6] F. P. Incropera, D. P. DeWitt, T. L. Bergman, and A. Lavine, *Fundamentals of heat and mass transfer*, 7th ed. Wiley, 2011.
- [7] B. R. Munson, D. F. Young, and T. H. Okiishi, *Fundamentals of fluid mechanics*, 7th ed. Wiley, 2013.
- [8] M. F. Modest, *Radiative heat transfer*, 3rd ed. Academic Press, 2013.
- [9] W. Wagner and A. Pruss, *The IAPWS industrial formulation 1997 for the thermodynamic properties of water and steam*. International Association for the Properties of Water; Steam (IAPWS), 1997.
- [10] F. M. White, *Fluid mechanics*, 8th ed. McGraw-Hill, 2016.
- [11] Crane Co., *Flow of fluids through valves, fittings, and pipe (technical paper no. 410)*, 25th ed. Crane Company, 2018.
- [12] P. K. Swamee and A. K. Jain, "Explicit equations for pipe-flow problems," *Journal of the Hydraulics Division*, vol. 102, no. 5, pp. 657–664, 1976.